CORROSION DAMAGE EVOLUTION OF A UNIDIRECTIONAL PIT

A Thesis

Presented to

The Graduate Faculty of The University of Akron

In Partial Fulfillment

of the Requirements for the Degree

Master of Science

John Motley McKinnon

August, 2016

CORROSION DAMAGE EVOLUTION OF A UNIDIRECTIONAL PIT

John Motley McKinnon

Thesis

Approved:

Advisor
Dr. Curtis Clemons

Faculty Reader
Dr. Gerald Young

Faculty Reader
Dr. Kevin Kreider

Department Chair
Dr. Timothy Norfolk

Accepted:

Dean of the College
John Green

Dean of the Graduate School
Dr. Chand Midha

Date

ABSTRACT

A three-stage, unidirectional pit growth model, from initiation to stable growth and repassivation as the bulk potential is decreased, is developed. Stage I models metastable pit growth under ohmic control and a constant current density. Here it is assumed that the pit is covered by a semi-permeable oxide layer. Stage I is terminated when the metal concentration reaches its saturation limit at which time the pit cover instantaneously bursts. Stage II models the stable pit growth under diffusion control and the formation of a salt film at the bottom of the pit. During Stage II the bulk potential is decreased at a specified scan rate. When the bottom pit potential reaches the transition potential, Stage III begins. Here we model the pit growth under ohmic control, for a prescribed polarization curve, until the metal repassivates as the potential is decreased. The governing system of equations for each stage is solved numerically to determine the potential drop, and the concentrations of sodium, chloride, and metal ions within the pit. The pit depth as a function of time is determined from Faraday's Law in Stages I and III, and from a mass balance at the electrolyte/metal interface in Stage II. The cumulative pit depth is fit to a power law model that is used in existing Markov models for pit initiation and growth, and is compared with experimental pit depths for stainless steel in seawater.

ACKNOWLEDGEMENTS

I would like to thank Drs. Young, Clemons, and Kreider for their incredible amount of encouragement and help that they have offered me during the creation of this document. I will never forget the meetings that we had each week, during which the work environment that they provided was very enjoyable and the humor they provided was unforgettable. I would also like to thank Abigail Cosgriff for her support during times that I felt stressed.

TABLE OF CONTENTS

Page

LIST OF TABLES

LIST OF FIGURES

CHAPTER I

INTRODUCTION

1.1 Pitting Corrosion and Corrosion Cells

Pitting corrosion is the process by which a metal has an accelerated dissolution of ions in a localized area on its surface [1]. A corrosion cell must be present in order for corrosion to occur on a metal. A corrosion cell is comprised of four key elements: an anodic region, a cathodic region, an ionic path, and an electron path. The anodic region is on the surface of the metal where an oxidation reaction occurs of the form

$$Me \rightleftharpoons Me^{n+} + ne^{-}, \tag{1.1}$$

which describes the release of n electrons. For our unidirectional pit model, we assume that this dissolution only takes place at the bottom of the pit, and not along the walls. The cathodic region is on the surface of the metal where a reduction reaction takes place. In particular, we are interested in the reduction of oxygen into hydroxide anions in the reaction

$$O_2 + 2H_2O + 4e^{-} \rightharpoonup 4OH^{-}. \tag{1.2}$$

An ionic pathway provides the necessary ionic transport processes for electrochemical reactions to take place. This ionic transport is any combination of diffusion, migration and convection of the ions. Note that the anode is the location where electrons are produced, and the cathode is where electrons are consumed. This constant exchange of electrons creates the electron path between the anode and the cathode. The oxidation and reduction reactions (1.1) and (1.2) are followed by a hydrolysis equilibrum reaction [2] in the form

$$Me^{n+} + H_2O \rightleftharpoons Me(OH)^{(n-1)+} + H^+ \tag{1.3}$$

where equilibrium is reached fairly quickly. It is important to note that (1.3) will give the minimum degree of acidification that is expected to be found inside the pit. We also assume [2] that the aggressive anion salts act as a supporting electrolyte for the ionic species that are formed in reactions (1.1) and (1.3) through electrolysis of sodium chloride

$$NaCl \rightarrow Na^+ + Cl^-. \tag{1.4}$$

1.2 Pit Initiation, Pit Growth and Mechanisms of Pitting

Many metals possess passive films, which are naturally occuring thin oxide layers that grow on their surface and greatly inhibit the process of pitting corrosion. In this section, we focus on the process of how pits initiate on passive metals (metals

with a passive film), how they exhibit metastable and stable growth, and the most important mechanisms that control their pitting process.

While it is not entirely known exactly how pitting corrosion is initiated on a passive metal, many important observations have given insight into the pitting process. In order for a pit to initiate, the passive film must break down and an aggressive chemistry must develop locally at the site of attack. A breakdown in the passive film is almost always due to either a chemical or physical imperfection of its crystalline structure. This means that attacks will typically occur on a crystal grain, grain boundary, flaw, or a place of mechanical damage or dislocation. [1, 3] The development of an aggressive chemistry is due to a high concentration of anion species, most frequently chloride and the strength of damage due to pitting varies directly with the logarithm of the chloride concentration [4]. If oxidizing agents are included into the solution of chloride ions, then the potential inside the pit increases which leads to the chemistry becoming even more aggressive and the damage more severe [1].

After a pit initiates there are many factors that control whether or not the pit will continue to grow in a stable fashion, or if it will quickly die. One very important quantity that controls pit propagation is the potential drop within the pit. It is widely known in the literature [1] that there is a critical potential known as the pitting potential E_{Pit} which defines the minimum potential that allows for the required local acidification in order to achieve stable growth. If the potential is lower than E_{Pit}, then pitting events are still possible but they are very short lived

due to being unable to maintain the local chemistry; these are known as metastable pits [4]. Note that the value of E_{Pit} is fixed for a particular metal in a prescribed environment and higher values of E_{Pit} indicate the metal is more resistant to pitting. Certain metal alloys and stainless steels are used in a wide variety of applications specifically because they tend to have thicker passive layers attributing to higher values of E_{Pit} than pure metals. In particular, stainless steels are used in water and sewage treatment equipment, for transport applications such as ship containers and chemical tanks, and for medical applications such as surgical equipment [5].

Because the stability of a pit is directly related to the pitting potential, it is important to understand the electrochemical factors that fix the value of E_{Pit}. These factors have been studied extensively in the literature [1]. In particular, the value of E_{Pit} is dependent upon both the aggressive and non-aggressive anion concentrations, the external pH, weak acid salts, and alloying elements in the metal [2]. According to results by Galvele [2] the pitting potential decreases in an amount directly proportional to the logarithm of aggressive anion (chloride) concentration. These results show the importance of anion concentration on the stability of pit growth. A higher chloride concentration will decrease the pitting potential and thus make it easier to maintain stable growth in the pit.

Pit stability is also related to the maximum pit depth inside the pit. Galvele's main result [2] was to discuss how a critical value of the factor xi, where x is the pit depth and i is the current density, corresponds to a critical pH level within a pit. By plotting various ionic concentrations as a function of xi he concludes that by knowing

the current density and total pit depth of one particular pit, the correct value of pH inside that particular pit can then be predicted. Additionally, if a particular change in concentration is needed for a given pit depth, the required current density can then be calculated. Note that Frankel states [1] that it is likely the case that the chloride concentration is a more important factor to consider in order to predict pit stability, rather than the critical pH as in the focus of Galvele.

The idea of metastable pits is particularly important to us when building our pit growth model, because metastable pits are able to transition into stable pits under certain conditions. Metastable pits are generally considered [1] to be pits that grow to be about $1\,\mu m$ in size and have a lifetime that is at most a few seconds. They are characterized by the presence of a pit cover; a semi-permeable oxide layer that forms on its surface. When a metastable pit transitions into a stable pit, the cover will burst instantaneously and there is a sudden drop in the current density. For this transition to occur, the applied potential must be greater than E_{Pit} and the current density is large enough for the metal concentration to reach a critical level of saturation [1]. This causes a building osmotic pressure of the metal ions and eventually a rupture in the cover, at which point pit growth will continue. According to Frankel [6] the precipitation of a salt film during the process of metastable growth is required for the pit to ultimately become stable. It was suggested by Vetter and Strehblow [7] that a resistive layer between the passive surface and the active pit bottom is required for growth of the pit to occur. The pit cover will provide the needed resistance during metastable growth, and the formation of a salt film at the pit bottom allows the pit

to become stable [6] so it can continue growing after the oxide layer has ruptured. The added resistance provided by the salt film also explains why there is a sudden drop in the current density at the moment that the cover breaks (since in that instant of time the potential and pit depth remain fixed).

Before we discuss the process by which a metal repassivates, we first describe two classifications of corrosion and their relationship to metastable and stable pitting. These are ohmic controlled corrosion and diffusion controlled corrosion. In ohmic controlled corrosion, the current density i plays an important role in the chemistry of the corrosion process through Ohm's Law in the relationship $V = iR$, where V is the potential and R is the (electrochemical) resistance. Ohm's Law shows us that if the current is increased, then the required resistance to achieve a fixed value of potential decreases (and hence the required pit depth also decreases). Thus, pits with large current densities do not need to be as deep as pits with smaller current densities in order to reach the pitting potential and become stable. It is for this reason that metastable growth can be described as an ohmic controlled corrosion process.

After a metastable pit transitions into being a stable pit, the pit is governed by diffusion controlled corrosion. When this happens, the pit enters a steady state growth process (multiple steady states may be possible for a single pit) where the dissolution rate of the metal ions at the interface exactly matches the diffusion rate of ions away from the surface [8]. This is mathematically interpreted as a mass balance of the two fluxes, and is described in more detail in the next chapter.

It is important to note that not every pit will stop growing (repassivate). In order to repassivate, the anodic and cathodic current densities in the pit must decrease [9] enough that it reaches a small, critical value known as the repassivation value i_{RP}. This will occur at a specific potential value E_{RP}. Thus, the pit chemistry is the determining factor that allows for a pit to either continue growing, or eventually shut down. If the environment of the pit allows for the potential to change very little from the bulk value E_B, then there is no limitation on the cathodic and anodic current and the pit is allowed to grow indefinitely. If however, the environment allows for a changing value of E_B, then the current density is limited and the pit will repassivate. Our model will focus specifically on pits that will eventually repassivate. For the purposes of simplifying the mathematics in our model, we will simply assume that the cathodic current and anodic current are always equal and we will only be concerned with anodic limitations.

According to Anderko [10], a pit that is undergoing stable growth will begin to repassivate when a metal oxide layer starts to form between the metal halide (salt) layer and the bottom of the pit. It is assumed that the oxide layer grows as the halide layer shrinks and the dissolution rate of the metal through the oxide layer is slower than through the halide layer. At the moment that the metal begins to repassivate, the potential takes on the transition value E_T. When there is enough ohmic drop for the metal to become passive, so the oxide layer is large enough that metal ions can no longer pass through, the potential has reached the repassivation value E_{RP}. During the repassivation process, Anderko [10] assumes that the current density decreases

as a function of the potential, so the current density is written as $i(E)$. Because repassivation depends upon the resistivity of the oxide layer and hence the ohmic drop in the pit, we say that the process is ohmic controlled.

We now summarize some of the most important assumptions and simplifications in current pit growth models in localized corrosion. If the reader wishes for a more extensive review of the relevant literature, the reader is referred to [11]. Most pitting and crevice models that wish to predict the damage h as a function of time t employ a one-dimensional approximation [2, 4, 8], so that the width of the crevice mouth is much smaller than the total depth h, or that for a cylindrical pit the radius r is much smaller than h. More recent models have been developed that predict the concentration field and the damage for two dimensional pits. However, these two dimensional models are much more computationally burdensome, and a solution must be found numerically using highly sophisticated techniques such as the combined level set and finite element method as presented in [12]. The model becomes much more complex when hydrolysis reactions are considered, which is why they are very frequently neglected [2, 8, 12] so that the only species considered are Fe^{2+}, Na^{+} and Cl^{-}. An additional simplification made to pit growth models is to assume that the concentration of ions in the pit is in steady state [4, 12, 13]. The basis of this argument is that the the velocity of the interface is so slow compared to the diffusion rate of the ions that the concentration in the pit undergoes steady flow [11]. The validity of this assumption is discussed in more depth in our model description in Chapter 2. One final simplification that is often made [4, 8, 13, 14], is that electromigration can

be neglected in the diffusion controlled regime. This detail is also discussed further in Chapter 2. The following is a list of assumptions we make for simplification of the model:

1. Hydrolysis reactions are neglected in a steel metal so we only consider the species Fe^{2+}, Na^{+} and Cl^{-}.

2. We only consider pits with width w and depth h such that $w << h$ so we may use a thin domain asymptotic expansion and pit growth is unidirectional.

3. The solid domain is homogeneous and the concentration of metal ions is a constant value $C = C_{solid}$ at all time [12].

4. Mass transport can be due to diffusion or electromigration from a potential gradient; however, advection is neglected.

5. The concentration of ions within the electrolyte is in steady state. Here bulk reactions are assumed to be fast and hence, the system is in equilibrium.

6. Electromigration can be neglected in the diffusion controlled regime, so that each ionic species is a linear function of pit depth.

Our pit model, which is the focus of this paper, consists of three separate stages of pit growth that describe how a single pit grows in time beginning with its birth, where it exhibits metastable growth, and ending with its death at the point that the metal repassivates. Our Stage I characterization is based on the description of metastable growth as presented by Frankel et al. [15]. According to Frankel et

al., the current for hemispherical pits during ohmic controlled metastable growth was found to increase with the square of the radius, and the IR drop was approximately constant, leading to a constant current density and a linear growth rate. Laycock [4] has shown that a pit cover will burst after the concentration reaches a certain fraction of its saturation limit, which is the minimum required value in order to maintain stable growth. Therefore, we end Stage I metastable growth and begin Stage II stable growth once the metal concentration reaches the critical value. Our Stage II characterization is based upon the numerous papers [4, 8, 13, 14] that have experimentally described transitions from ohmic controlled metastable growth to diffusion controlled stable growth. In each of these studies, the current density during stable growth was found to be dominated by the diffusion gradient, leading to $i_L \propto \frac{1}{h}$ so that $h \approx t^{1/2}$ by Faraday's Law. Further, a salt film forms in the transition from Stage I to Stage II. We assume this formation is instantaneous and do not model this transient behavior that occurs between Stages I and II. Our Stage III characterization is based upon our previous discussion of repassivation according to Anderko [10], where pit repassivation begins at the potential $E = E_T$, ends at $E = E_{RP}$, and the current density is a function of potential $i(E)$. Similar to the neglect of any transient behavior between Stages I and II, we also neglect transients between Stages II and III. Our model consists of the following three quasi-steady stages:

- Stage I - Ohmic controlled metastable growth that varies linearly in time. The current density is constant and large and we transition to Stage II once the metal concentration reaches a critical percent of the saturation value C_{sat}.

- Stage II - Diffusion controlled stable growth that varies according to the square root of time. We transition to Stage III when the potential reaches the transition potential $E = E_T$.

- Stage III - Ohmic controlled stable growth where the depth will asymptotically reach its maximum value at a rate that is slower than the square root of time. The current density is chosen to be a decreasing function of potential. Growth ends when the repassivation potential E_{RP} is reached.

A more detailed explanation for the growth rates of each of the three stages is given in the next chapter where we describe each stage of the model in more depth. As we describe each of the three stages of the pit growth model, we refer to the polarization curve in Figure 1.1, which gives the relatonship between the potential E and the current density i. The theoretical values of the potential and current density used to define the polarization curve are chosen to match the data given in Srinivisan [16] and are shown in Table 1.1 In solving the problem numerically, we choose the repassivation values E_{RP} and i_{RP} to be the same as the stated theoretical values; however the diffusion limiting values i_T and E_T are calculated and then compared to Table 1.1 This is discussed further in Chapter 3 when we describe the numerical implementation.

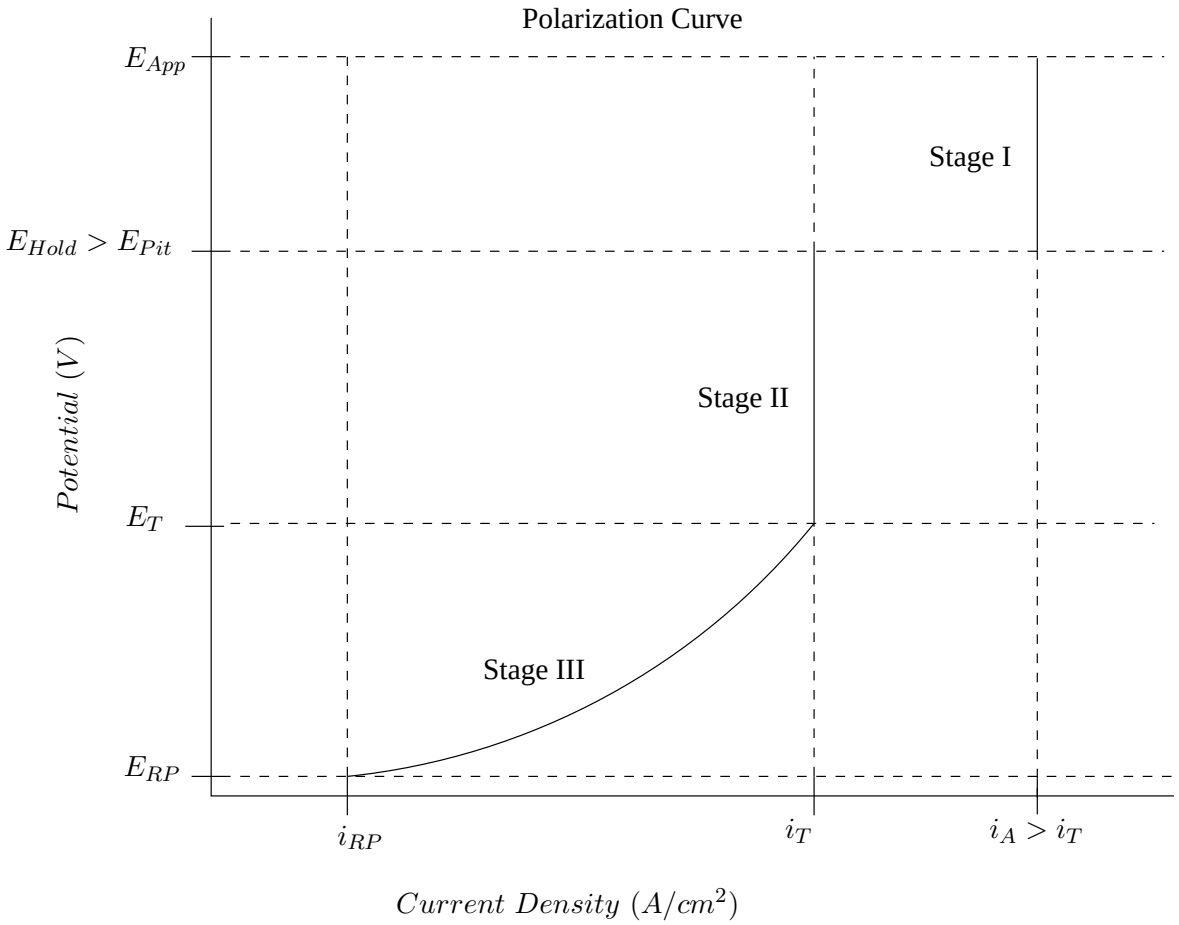

Figure 1.1: The polarization curve for each of the three stages in the growth model.

Table 1.1: Polarization curve values.

Variable Name	Description	Numerical Value	Unit
E_{App}	Applied Potential	0.510	V
E_{Hold}	Potential Value During Potentiostatic Hold	0.45	V
E_T	Transition Potential	0.025	V
i_T	Transition Current Density	0.50	$\frac{A}{cm^2}$
E_{RP}	Repassivation Potential	-0.16	V
i_{RP}	Repassivation Current Density	3.0e-5	$\frac{A}{cm^2}$

CHAPTER II

MODEL DESCRIPTION

2.1 Geometry of the Problem and the Governing Equation

Consider the cross section of a pit (side view) where the width is w and depth h. In each of the three stages we set the top of the pit as the location $z = 0$ and at the bottom of the pit we have $z = h(x,t)$ so the pit depth varies as a function of time and width. Assuming that $w << h$, then we may use a thin domain asymptotic expansion leading to a unidirectional growth model with $z = h(t)$ only. A diagram of the domain of the problem is shown in Figure 2.1.

The ion flux $\vec{J_j}$ is represented in terms of the concentration C_j corresponding to the species j of ions and in terms of the potential E as

$$\vec{J_j} = -D_j(\vec{\nabla}C_j) - n_j\alpha D_j C_j(\vec{\nabla}E). \tag{2.1}$$

Here, D_j is the diffusivity and n_j represents the charge of the species where n_j is (+) for an anion and n_j is (-) for a cation. The parameter α is defined by

$$\alpha = \frac{F}{RT} \tag{2.2}$$

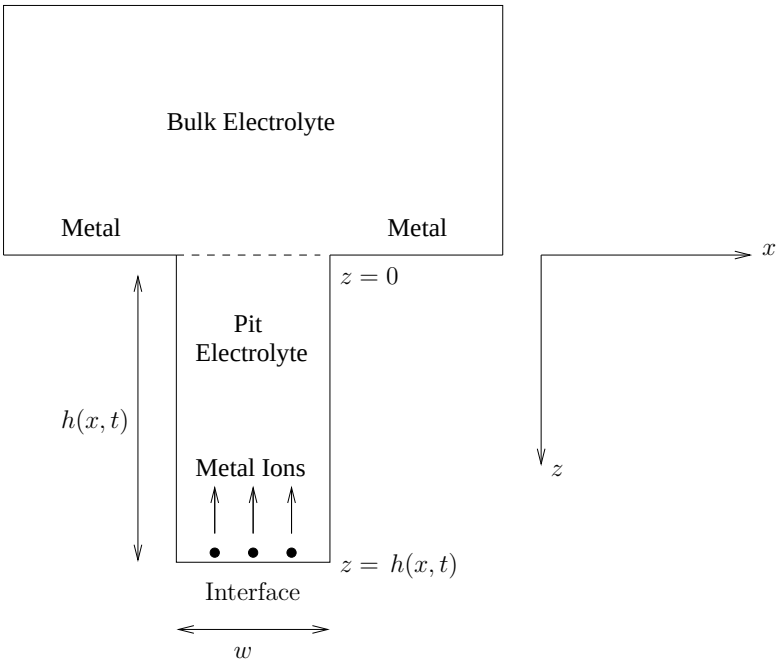

Figure 2.1: The domain of the problem.

where F is Faraday's Constant, R is the universal gas constant, and T is the temperature in kelvin. The first term in (2.1) represents the diffusion of ions through a concentration gradient, and the second term represents the migration of ions as the result of an electric field due to a potential gradient. Note that as z increases, the potential goes from high potential at the cathode to low potential at the anode, so that $\vec{\nabla}E < 0$. Also note that as z increases, the concentration changes from low concentration to high concentration so $\vec{\nabla}C_j > 0$.

The continuity equation gives

$$\frac{\partial C_j}{\partial t} + \vec{\nabla} \cdot \vec{J}_j = s^{(+)} - s^{(-)} \tag{2.3}$$

with $s^{(+)}$ representing a source and $s^{(-)}$ representing a sink. Assuming that the system is in equilibrium, we have

$$\vec{\nabla} \cdot \vec{J}_j = -\frac{\partial C_j}{\partial t}. \tag{2.4}$$

In each of the three stages of pit growth, we need to find the potential $E(z,t)$ in the pit. The outward normal points in the positive z direction, so (2.4) is equivalent to the governing equation

$$\frac{\partial \vec{J}_j}{\partial \hat{n}} = \frac{\partial}{\partial z}\left[D_j \frac{\partial C_j}{\partial z} + n_j \alpha D_j C_j \frac{\partial E}{\partial z}\right] = -\frac{\partial C_j}{\partial t}. \tag{2.5}$$

The growth rate at the bottom of the pit is governed by Faraday's Law

$$\frac{\partial h}{\partial t} = \frac{i_A MW}{2\rho F}. \tag{2.6}$$

Here, $\rho = 7.92\,\frac{g}{cm^3}$ is the density of the steel alloy [16] and $MW = 55.85\,\frac{g}{mol}$ is its molecular weight [16]. We define the non-dimensional time $\bar{t}$ as

$$\bar{t} = \frac{t}{t_{trans}}, \tag{2.7}$$

where

$$t_{trans} = \frac{2\rho F h}{i_A MW} \tag{2.8}$$

is the time scale for dissolution of metal at the bottom of the pit. The non-dimensional diffusion equation is then given by

$$\frac{\partial}{\partial \bar{z}}\left[\frac{\partial \bar{C}_j}{\partial \bar{z}} + \bar{C}_j \frac{\partial \bar{E}}{\partial \bar{z}}\right] = -\frac{1}{t_{trans}} \frac{h^2}{D_j(1+|n_j|\alpha E)} \frac{\partial \bar{C}_j}{\partial \bar{t}}, \tag{2.9}$$

where $\bar{z} = \dfrac{z}{h}$ and $\bar{E} = \dfrac{E}{E_B}$. The quantity

$$t_{diff} = \frac{h^2}{D_j(1+|n_j|\alpha E)} \tag{2.10}$$

represents the time scale for the diffusion of ions in the pit. Note that after non-dimensionalization, the quantity $|n_j|\alpha E_B$ is O(1), so that all terms on the transport side of (2.9) are $O(1)$. Therefore, the non-dimensional group

$$\epsilon = \frac{t_{diff}}{t_{trans}} \tag{2.11}$$

will control the size of the time derivative. Assuming that h, D_j, and i_A have sizes that are no larger than $100\,\mu m$, $1.0 \times 10^{-5}\, cm^2/s$ and $5.0\, A$ respectively, the quantity t_{trans} is much slower than t_{diff} and we have $\epsilon << 1$. When we keep terms of $O(1)$ and neglect terms of $O(\epsilon)$, the diffusion equation

$$\frac{\partial}{\partial \bar{z}}\left[\frac{\partial \bar{C}_j}{\partial \bar{z}} + \bar{C}_j \frac{\partial \bar{E}}{\partial \bar{z}}\right] = -\epsilon \frac{\partial \bar{C}_j}{\partial \bar{t}}, \tag{2.12}$$

is equivalent to the quasi-steady state equation

$$\vec{\nabla} \cdot \vec{J}_j = 0. \tag{2.13}$$

We use the term quasi-steady because the pit depth is still increasing with time. Thus, the diffusion equation can be reduced to the quasi-steady state (dimensional) equation

$$\frac{\partial}{\partial z}\left[D_j \frac{\partial C_j}{\partial z} + n_j \alpha D_j C_j \frac{\partial E}{\partial z}\right] = 0, \tag{2.14}$$

which can be used to determine the potential inside the pit $E(z,t)$. Integration of (2.14) with respect to z gives

$$\frac{\partial C_j}{\partial z} + n_j \alpha C_j \frac{\partial E}{\partial z} = J = constant. \tag{2.15}$$

For a non-reactive species at the electrolyte/metal interface, $J = 0$ so that

$$\frac{\partial C_j}{\partial z} + n_j \alpha C_j \frac{\partial E}{\partial z} = 0. \tag{2.16}$$

Separation of variables and integration with respect to z gives an expression for the concentration C_j as a function of potential E as follows. Note that because the potential $E = E(z,t)$ is a function of pit depth and time, the concentration $C_j = C_j(z,t)$ is also a function of pit depth and time. Here, the index j may refer to either the concentration of metal ions $C = [Fe^{2+}]$, or the concentration of the sodium

cations $\left[Na^+\right]$ or chloride anions $\left[Cl^-\right]$. From this point forward, we suppress the time dependence of $E(z,t)$ and similar terms so that $E(z,t)$ is to be interpreted as $E(z)$ for the remainder of the document. The coefficients A_j are found to be

$$A_j = C_j(0)e^{n_j\alpha E_B}, \tag{2.17}$$

where $E(0) = E_B$ is the potential in the bulk electrolyte and $C_j(0)$ refers to the bulk concentration of species j. Note that the bulk potential E_B is a function of time because it is linearly stepped in time during Stages II and III. So the concentration is written as

$$C_j(z) = C_j(0)e^{-n_j\alpha[E(z)-E_B]}. \tag{2.18}$$

Hence, the concentrations of the sodium cations and the chloride anions are written as

$$\left[Cl^-\right] = Cl^-_{bulk}e^{-\alpha[E-E_B]}, \tag{2.19}$$

$$\left[Na^+\right] = Na^+_{bulk}e^{\alpha[E-E_B]}. \tag{2.20}$$

The electroneutrality condition gives an expression for the concentration C_j as a function of E,

$$-n_j\left[C_j\right] + \left[Na^+\right] - \left[Cl^-\right] = 0. \tag{2.21}$$

Therefore when we drop the j and use $n_j = -2$ for the iron concentration C then

$$C(z) = \frac{1}{2}\left[Cl^-_{bulk}e^{-\alpha[E(z)-E_B]} - Na^+_{bulk}e^{\alpha[E(z)-E_B]}\right], \tag{2.22}$$

where the derivative is

$$\frac{\partial C}{\partial z} = -\frac{\alpha}{2}\left(\frac{\partial E}{\partial z}\right)\left[Cl^-_{bulk}e^{-\alpha[E-E_B]} + Na^+_{bulk}e^{\alpha[E-E_B]}\right]. \tag{2.23}$$

2.2 Stage I Model Description

In Stage I, we assume that the growth of the pit is metastable, and is ohmically controlled so the pit growth depends upon the current density at the bottom of the pit. We assume that there is a semi-permeable membrane with a mass transport coefficient $0 < k < \infty$ to allow passage of metal cations into the bulk at the top of the pit. A diagram of the model in Stage I is shown in Figure 2.2.

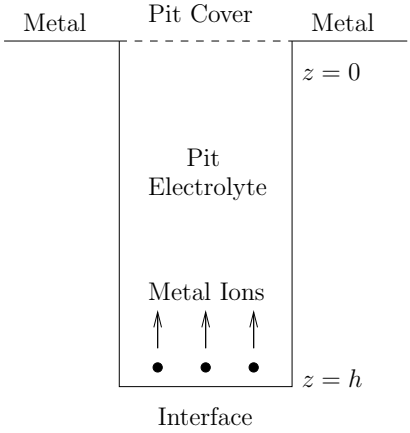

Figure 2.2: The Stage I pit growth model.

At the pit cover $z = 0$, the net flux of metal ions is given by

$$-D\frac{\partial C}{\partial z} + 2\alpha DC\frac{\partial E}{\partial z} = -k(C - C_{bulk}), \qquad \text{at } z = 0, \tag{2.24}$$

where C_{bulk} is the metal concentration in the bulk. Here, the flux is proportional to the difference in concentration $C - C_{bulk}$, where the direction of transport is from the pit interior to the bulk. Because the concentration at the pit cover $C(z = 0)$ is much smaller than the concentration at the pit bottom $C(z = h)$, the electromigration term is neglected and the boundary condition becomes

$$-D\frac{\partial C}{\partial z} = -k(C - C_{bulk}), \qquad \text{at } z = 0. \tag{2.25}$$

At the bottom of the pit, there is a mass balance between the metal ion flux and the current, so we have

$$D\frac{\partial C}{\partial z} - 2\alpha DC\frac{\partial E}{\partial z} = \frac{i_A}{2FC_{Solid}}(C_{Solid} - C), \qquad \text{at } z = h(t) \tag{2.26}$$

where C_{solid} is the metal concentration at the solid interface. Note that the direction of transport is from the solid to the electrolyte. As we have stated in the previous section, the pit depth grows in time according to Faraday's Law in (2.6). We take the anodic current density i_A to be a constant so the pit depth h is a linear function of time. Equation (2.6) can be used to determine the damage h at each time step

by integration. When we substitute the metal concentration (2.22) and its derivative (2.23) into the governing equation (2.14) where $n_j = -2$ for iron, we have the second order ODE written only in E,

$$\frac{\partial}{\partial z}\Bigg(-\frac{\alpha}{2}\frac{\partial E}{\partial z}\left[Cl_{bulk}e^{-\alpha[E-E_B]} + Na_{bulk}e^{\alpha[E-E_B]}\right] - \alpha\frac{\partial E}{\partial z}\left[Cl_{bulk}e^{-\alpha[E-E_B]} - Na_{bulk}e^{\alpha[E-E_B]}\right]\Bigg) = 0. \quad (2.27)$$

Combining terms and simplifying (2.27) we have

$$\frac{\partial}{\partial z}\left(\frac{\partial E}{\partial z}\left[-3Cl_{bulk}e^{-\alpha[E-E_B]} + Na_{bulk}e^{\alpha[E-E_B]}\right]\right) = 0. \quad (2.28)$$

Distrubuting the derivative in (2.28) yields

$$\left[-3Cl_{bulk}e^{-\alpha[E-E_B]} + Na_{bulk}e^{\alpha[E-E_B]}\right]\frac{\partial^2 E}{\partial z^2} + \alpha\left[3Cl_{bulk}e^{-\alpha[E-E_B]} + Na_{bulk}e^{\alpha[E-E_B]}\right]\left(\frac{\partial E}{\partial z}\right)^2 = 0. \quad (2.29)$$

In order to simplify notation, we write (2.29) in terms of the functions $A(z)$ and $B(z)$ to give the final form of our governing equation:

$$\begin{cases} A(z)\dfrac{\partial^2 E}{\partial z^2} + B(z)\left(\dfrac{\partial E}{\partial z}\right)^2 = 0, \\ A(z) = -3Cl^-_{bulk}e^{-\alpha[E-E_B]} + Na^+_{bulk}e^{\alpha[E-E_B]}, \\ B(z) = \alpha\left[3Cl^-_{bulk}e^{-\alpha[E-E_B]} + Na^+_{bulk}e^{\alpha[E-E_B]}\right]. \end{cases} \quad (2.30)$$

Using both (2.22) and (2.23) in the boundary conditions (2.25) and (2.26), we have two conditions for the potential E,

$$\alpha D\left(\frac{\partial E}{\partial z}\right)\left[Cl^-_{bulk}e^{-\alpha[E-E_B]}+Na^+_{bulk}e^{\alpha[E-E_B]}\right]$$
$$=k\left[2Na^+_{bulk}-Cl^-_{bulk}e^{-\alpha[E(z)-E_B]}+Na^+_{bulk}e^{\alpha[E-E_B]}\right],\quad \text{at } z=0. \quad (2.31)$$

$$\frac{\alpha}{2}\left(\frac{\partial E}{\partial z}\right)\left[-3Cl^-_{bulk}e^{-\alpha[E-E_B]}+Na^+_{bulk}e^{\alpha[E-E_B]}\right]$$
$$=\frac{i_A}{4FC_{solid}D}\left[2C_{solid}-Cl^-_{bulk}e^{-\alpha[E(z)-E_B]}+Na^+_{bulk}e^{\alpha[E-E_B]}\right],\quad \text{at } z=h(t). \quad (2.32)$$

Experiments have shown [4] that a pit cover will burst after the concentration reaches a certain fraction of its saturation limit, which is the minimum required value in order to maintain stable growth. This minimum value has been commonly accepted to be roughly between 60-80% [8, 17]. We estimate this fraction conservatively, and assume the stopping condition in our Stage I model when we transition to stable growth is when the concentration reaches 60% of the saturation limit, so $C = \gamma C_{sat}$, with $\gamma = 0.6$ at which point we no longer update the damage.

2.3 Stage II Model Description

After reaching saturation, the pit cover at $z = 0$ in Figure 2.2 instantaneously ruptures due to the building osmotic pressure of the metal ions. There is a decrease in current

and potential and we transition to the Stage II model where the pit exhibits diffusion controlled stable growth. The defining characteristic for stable growth of a pit is the formation of a metal halide salt layer at the interface between the metal and the electrolyte solution. As the pit grows deeper in time, the salt layer becomes thicker. This halide layer increases the resistance in the pit solution. Mathematically, this is incorporated into our model by linearly decreasing the bulk potential E_B over time.

The governing equation that we are interested in solving is still (2.14), however the boundary conditions are different. Because the pit cover is no longer present, it is not able to act as a resistive layer to the flow of ions, so the boundary condition at the top of the pit is

$$E = E_B \text{ at } z = 0. \tag{2.33}$$

The potential is fixed at the value of the bulk electrolyte. The concentration at the pit bottom stays fixed, so using $C = \gamma C_{sat}$ in (2.22) gives

$$\gamma C_{sat} = \frac{1}{2}\left[Cl^-_{bulk} e^{-\alpha[E(z)-E_B]} - Na^+_{bulk} e^{\alpha[E(z)-E_B]}\right] \text{ at } z = h. \tag{2.34}$$

Equation (2.34) is used to solve for the potential at the bottom of the pit, $E(z = h)$, and is equivalent to

$$Na_{bulk} e^{2\beta} - 2\gamma C_{sat} e^{\beta} + Cl_{bulk} = 0, \tag{2.35}$$

where $\beta = \alpha[E(z=h) - E_B]$. The two roots of the quadratic equation are

$$\xi_{\pm} = \frac{-\gamma C_{sat} \pm \sqrt{\gamma^2 C_{sat}^2 + Na_{bulk} Cl_{bulk}}}{Na_{bulk}} = e^{\beta}, \tag{2.36}$$

and the potential at the bottom of the pit is

$$E(z=h) = \frac{1}{\alpha} ln(\xi_+) + E_B. \tag{2.37}$$

The positive root is taken to ensure that the potential drop ΔE is positive. In particular, we have

$$\Delta E = E_B - E(z=h) = -\frac{1}{\alpha} ln(\xi_-). \tag{2.38}$$

Note that $E(z=h)$ and ΔE are both constants that depend upon the bulk values Na_{bulk} and Cl_{bulk} as well as the saturation level of the metal C_{sat}. In addition, the potential at the pit bottom depends upon the bulk potential E_B. The major conclusion is that the potential drop down the depth of the pit is fixed in Stage II. A diagram of the Stage II model is given in Figure 2.3.

Because the pit growth is diffusion controlled, the metal ion flux is the same as the dissolution rate of the metal at the bottom of the pit so we have that

$$D\frac{\partial C}{\partial z} - 2\alpha DC\frac{\partial E}{\partial z} = \frac{\partial h}{\partial t}(C_{solid} - \gamma C_{sat}) \text{ at } z = h(t). \tag{2.39}$$

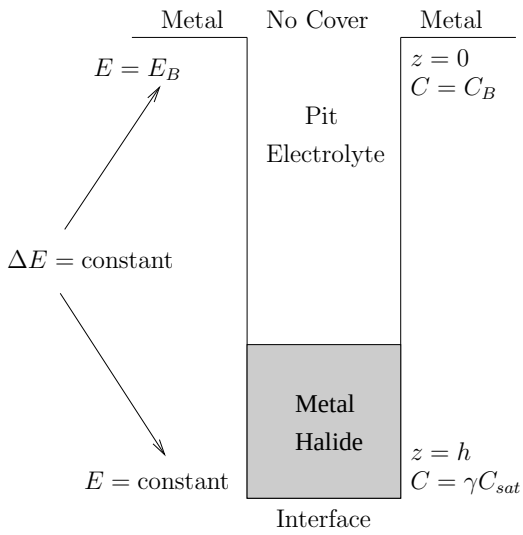

Figure 2.3: The Stage II pit growth model.

The growth rate of the pit is then given by

$$\frac{\partial h}{\partial t} = \frac{D}{C_{solid} - \gamma C_{sat}} \left(\frac{\partial C}{\partial z} - 2\alpha C \frac{\partial E}{\partial z} \right) \text{ at } z = h(t). \tag{2.40}$$

According to Moayad and Newman [13], and experiments conducted by Tester and Isaacs [18, 19], the current is dominated by the diffusion gradient for diffusion controlled pit growth where the bulk concentration of $NaCl$ is between $0.5 \times 10^{-4} \frac{mol}{cm^3}$ and $10 \times 10^{-4} \frac{mol}{cm^3}$. Issacs [19] argued that the potential has little effect on the current because the system is self-regulating. He states that any perturbations in the current that occur from stepping the potential will only occur for a short period of time, until the current returns to a value equal to the diffusion flux. This is consistent with our quasi-steady state assumption where all transients are fast compared to the dissolution rate. It follows that the electromigration term can be neglected in (2.40)

and the governing equation (2.14), so that we have $\frac{\partial^2 C}{\partial z^2} = 0$, and the growth rate can be simplified to

$$\frac{\partial h}{\partial t} = \frac{D}{C_{solid} - \gamma C_{sat}} \left(\frac{\partial C}{\partial z} \right) \text{at } z = h(t). \tag{2.41}$$

The concentration is linear, so

$$C(z) = a + bz. \tag{2.42}$$

The boundary conditions $C(0) = C_{bulk}$ and $C(z = h) = \gamma\, C_{sat}$ then give

$$C = C_{bulk} + \left(\frac{\gamma C_{sat} - C_{bulk}}{h} \right) z. \tag{2.43}$$

The derivative $\frac{\partial C}{\partial z}$ is given by

$$\frac{\partial C}{\partial z} = \left(\frac{\gamma C_{sat} - C_{bulk}}{h} \right), \tag{2.44}$$

and we have

$$\frac{\partial h}{\partial t} = \frac{D\left(\gamma C_{sat} - C_{bulk}\right)}{C_{solid} - \gamma C_{sat}} \frac{1}{h} \propto \frac{1}{h}. \tag{2.45}$$

It follows that

$$h\,dh \approx dt \implies h \propto t^{1/2}. \tag{2.46}$$

This fact allows us to assume that the overall damage profile in time can be fit using a power law as

$$h(t) = at^b. \tag{2.47}$$

The current density is not constant as we had assumed previously in Stage II, but is instead decreasing with pit depth. We refer to Chapter 3 for discussion on a method where we are able to use (2.45) together with Faraday's Law in (2.6) for calculating the diffusion limiting current density for Stage II.

A stable pit shuts down only if the pit has a limiting cathodic current density. Here, we make the assumption that the anodic and cathodic current densities are the same, and we simulate a limiting cathodic value by stepping the potential down along the polarization curve beginning at the potential value $E_B = E_{Hold} > E_{Pit}$ and ending at the transition potential $E = E_T$. Thus, our stopping condition for Stage II is for $E = E_T$. This is mathematically equivalent to the experimental process of scanning the potential with a scanning electrode procedure as performed by Srinivasan [16]. Prior to scanning, Srinivasan held the potential fixed and allowed the pit to drill to various specified depths. In order to match the polarization curve and to obtain

pit depths on the same order of magnitude as reported by Srinivisan, we have taken the same approach in our Stage II model. We hold the potential fixed and update the damage and concentration profiles until we reach close to $i_T = 0.50\, A/cm^2$. Our process that is used to step down the potential is described in more detail in Chapter 3.

2.4 Stage III Model Description

In the Stage III model, the pit begins to approach repassivation through ohmic controlled growth as in Figure 2.4. Because the pit cover is still gone in Stage III, we have

$$E = E_B \text{ at } z = 0. \tag{2.48}$$

Because the growth is ohmic controlled, the mass balance between the metal ion flux and the current gives

$$D\frac{\partial C}{\partial z} - 2\alpha DC\frac{\partial E}{\partial z} = \frac{i_A(E)}{2FC_{Solid}}(C_{Solid} - C), \qquad \text{at } z = h(t) \tag{2.49}$$

where we no longer assume that the anodic current density is constant as in Stage I, but now varies with potential. The growth of the pit is then

$$\frac{\partial h}{\partial t} = \frac{i_A(E)MW}{2\rho F}, \qquad \text{at } z = h(t). \tag{2.50}$$

Using (2.22) and (2.23) the boundary condition is

$$\frac{\alpha}{2}\left(\frac{\partial E}{\partial z}\right)\left[-3Cl^-_{bulk}e^{-\alpha[E(z)-E_B]}+Na^+_{bulk}e^{\alpha[E(z)-E_B]}\right]$$
$$=\frac{i_A(E)}{4FC_{solid}D}\left[2C_{solid}-Cl^-_{bulk}e^{-\alpha[E(z)-E_B]}+Na^+_{bulk}e^{\alpha[E(z)-E_B]}\right],\ \text{ at } z=h(t). \tag{2.51}$$

In Stage III, repassivation is begun at the transition value E_T where the metal oxide layer begins to form between the halide layer and the metal interface and repassivation has completed after the potential has been stepped down to the value E_{RP} at the pit bottom. The scanning process and the numerical implementation for our current density $i(E)$ using the polarization curve is described in more detail in the algorithm description in Chapter 3.

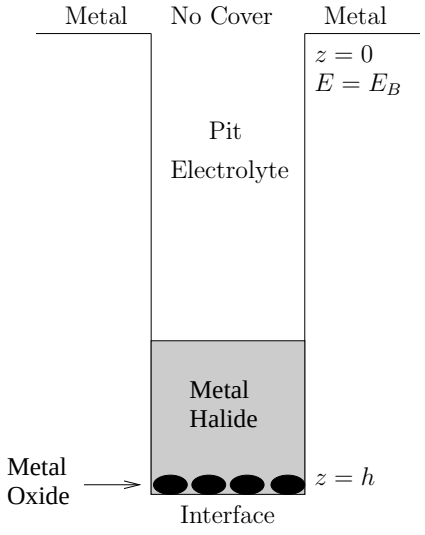

Figure 2.4: The Stage III pit growth model.

2.5 Quick Reference For Model Equations

Quick reference equations are given in terms of C and also in terms of E. The forms using C are easier to understand and manipulate from a conceptual point of view, and are listed first.

Governing Equation (In terms of C):

$$\frac{\partial}{\partial z}\left[D\frac{\partial C}{\partial z} - 2\alpha DC\frac{\partial E}{\partial z}\right] = 0.$$

Electroneutrality Condition:

$$C(z) = \frac{1}{2}\left[Cl^-_{bulk}e^{-\alpha[E(z)-E_B]} - Na^+_{bulk}e^{\alpha[E(z)-E_B]}\right].$$

Stage I Boundary Conditions (In terms of C):

$$-D\frac{\partial C}{\partial z} = -k(C - C_{bulk}), \qquad \text{at } z = 0,$$

$$D\frac{\partial C}{\partial z} - 2\alpha DC\frac{\partial E}{\partial z} = \frac{i_A}{2FC_{Solid}}(C_{Solid} - C), \quad \text{at } z = h(t),$$

$$\frac{\partial h}{\partial t} = \frac{i_A MW}{2\rho F}.$$

Stage II Concentration

$$C = C_{bulk} + \left(\frac{\gamma C_{sat} - C_{bulk}}{h} \right) z.$$

Stage II Boundary Conditions (In terms of C):

$$E = E_B, \qquad \text{at } z = 0,$$

$$C = \gamma C_{sat}, \qquad \text{at } z = h(t),$$

$$\frac{\partial h}{\partial t} = \frac{D\left(\gamma C_{sat} - C_{bulk}\right)}{C_{solid} - \gamma C_{sat}} \frac{1}{h}.$$

Stage III Boundary Conditions (In terms of C):

$$E = E_B, \qquad \text{at } z = 0,$$

$$D\frac{\partial C}{\partial z} - 2\alpha DC\frac{\partial E}{\partial z} = \frac{i_A(E)}{2FC_{Solid}}(C_{Solid} - C), \quad \text{at } z = h(t),$$

$$\frac{\partial h}{\partial t} = \frac{i_A(E)MW}{2\rho F}.$$

Here, the quick reference equations are given in terms of E. These are the equations that we will solve using MATLAB.

Governing Equation (In terms of E):

$$A(z)\frac{\partial^2 E}{\partial z^2} + B(z)\left(\frac{\partial E}{\partial z}\right)^2 = 0,$$

where

$$A(z) = -3Cl^-_{bulk}e^{-\alpha[E(z)-E_B]} + Na^+_{bulk}e^{\alpha[E(z)-E_B]},$$

and

$$B(z) = \alpha\left[3Cl^-_{bulk}e^{-\alpha[E(z)-E_B]} + Na^+_{bulk}e^{\alpha[E(z)-E_B]}\right].$$

Stage I Boundary Conditions (In terms of E):

$$\alpha D\left(\frac{\partial E}{\partial z}\right)\left[Cl^-_{bulk}e^{-\alpha[E(z)-E_B]} + Na^+_{bulk}e^{\alpha[E(z)-E_B]}\right]$$
$$= k\left[2Na^+_{bulk} - Cl^-_{bulk}e^{-\alpha[E(z)-E_B]} + Na^+_{bulk}e^{\alpha[E(z)-E_B]}\right], \quad \text{at } z = 0,$$

$$\frac{\alpha}{2}\left(\frac{\partial E}{\partial z}\right)\left[-3Cl^-_{bulk}e^{-\alpha[E(z)-E_B]} + Na^+_{bulk}e^{\alpha[E(z)-E_B]}\right]$$
$$= \frac{i_A}{4FC_{solid}D}\left[2C_{solid} - Cl^-_{bulk}e^{-\alpha[E(z)-E_B]} + Na^+_{bulk}e^{\alpha[E(z)-E_B]}\right], \quad \text{at } z = h(t),$$

$$\frac{\partial h}{\partial t} = \frac{i_A MW}{2\rho F}.$$

Stage II Boundary Conditions (In terms of E):

$$E = E_B, \qquad \text{at } z = 0,$$

$$E = \frac{1}{\alpha} ln(\xi_-) + E_B, \qquad \text{at } z = h(t),$$

where

$$\xi_- = \frac{\gamma C_{sat} - \sqrt{\gamma^2 C_{sat}^2 - Na_{bulk} Cl_{bulk}}}{Na_{bulk}},$$

$$\frac{\partial h}{\partial t} = \frac{D\left(\gamma C_{sat} - C_{bulk}\right)}{C_{solid} - \gamma C_{sat}} \frac{1}{h}.$$

Stage III Boundary Conditions (In terms of E):

$$E = E_B, \qquad at\ z = 0,$$

$$\frac{\alpha}{2}\left(\frac{\partial E}{\partial z}\right)\left[-3Cl_{bulk}^- e^{-\alpha[E(z)-E_B]} + Na_{bulk}^+ e^{\alpha[E(z)-E_B]}\right]$$

$$= \frac{i_A(E)}{4FC_{solid}D}\left[2C_{solid} - Cl_{bulk}^- e^{-\alpha[E(z)-E_B]} + Na_{bulk}^+ e^{\alpha[E(z)-E_B]}\right], \quad at\ z = h(t)$$

$$\frac{\partial h}{\partial t} = \frac{i_A(E) MW}{2\rho F}.$$

CHAPTER III

NUMERICAL IMPLEMENTATION AND ALGORITHM DESCRIPTION

3.1 Stage I Implementation

The spatial grid z is built using $N = 5001$ equally spaced points, z_m. The grid value $z_1 = 0$ is the location at the top of the pit and the value $z_N = h^{(n+1)}$ is the location at the bottom so the spatial domain is $z \in \left[0,\, h^{(n+1)}\right]$. Here $h^{(1)}$ is the scalar value of the total damage when the pit initiates (time step $n = 0$) and $h^{(n+1)}$ is the total damage at the nth time step. The time grid t is built using $n + 1$ equally spaced points so the time domain is $t \in [0,\, t_n]$. When we use separation of variables on (2.6) we obtain

$$h(t) = h(0) + \frac{i_A\, MW}{2\rho F} t, \tag{3.1}$$

which we discretize as

$$h^{(n+1)} = h^{(1)} + \frac{i_A\, MW}{2\rho F} n dt. \tag{3.2}$$

At each of the three stages in the model, the governing equation (2.30) is solved using 4th order Runge-Kutta (ode45 in MATLAB) to determine the potential. For each stage, we describe the algorithm that is used to determine the damage, potential and concentrations for all time. The following is a step by step implementation for our Stage I model:

1. Assuming the initial pit depth of $h^{(1)} = 1\,\mu m$, determine the potential $E(z)$ and its derivative $\dfrac{\partial E}{\partial z}$ when $t = 0$ by solving equation (2.30) subject to the boundary conditions (2.31) and (2.32).

2. For $t = 0$, determine the concentrations of sodium and chloride as well as the concentrations of the metal by using the solution for $E(z)$ in the electroneutrality condition (2.22). Determine the derivative $\dfrac{\partial C}{\partial z}$ using (2.23).

3. For time step n, update the damage $h^{(n+1)}$ by using (3.2) with $dt = 0.1$ second, and rebuild the z grid using N points in the new spatial domain $\left[0,\, h^{(n+1)}\right]$.

4. Use $h^{(n+1)}$ and the new z grid to repeat steps (1) and (2) at time step n.

5. Exit the time loop when $C = \gamma C_{sat}$.

A list of the parameters used in Stage I of the model are given in Table 3.1. We choose the bulk iron concentration to be the arbitrarily small value $C_{bulk} = 1.0 \times 10^{-5}\,\frac{mol}{cm^3}$ and the bulk chloride concentration to be $Cl_{bulk} = 6.0 \times 10^{-4}\,\frac{mol}{cm^3}$, which is consistent with the data set in Srinivasan et al. [16]. The bulk sodium concentration is obtained from the electroneutrality condition in (2.22) to be $Na_{bulk} = 5.8 \times 10^{-4}\,\frac{mol}{cm^3}$. The values for ρ, MW, C_{solid}, T, D, and E_B are also chosen to match the data in [16]. In particular, D is chosen so that our expression for the slope m of a graph of i_L versus $\frac{1}{h}$ matches the slope in [16]. The parameter γ is chosen based on a conservative estimate for the minimum fraction of saturation needed to maintain stable growth, as presented in [8, 17]. Our value for C_{sat} is based upon estimates of C_{sat} for 316L stainless steel according to Bright in [20]. Assuming that 316L stainless steel is comprised of 67.5 %

Fe, it has the saturation limit [20]

$$C_{sat(steel)} = \frac{C_{sat(iron)}}{0.675} = 1.48 C_{sat(iron)}. \tag{3.3}$$

According to Laycock et al. [14], at 23 °C the saturation limit of Fe^{2+} in $FeCl_2$ is $3.5{\times}10^{-3}\ \frac{mol}{cm^3}$. Therefore, we have $C_{sat(steel)} = 5.18 \times 10^{-3}\,\frac{mol}{cm^3}$, which is the value we choose for our saturation limit.

Table 3.1: Stage I Model Parameters (Baseline)

Variable Name	Description	Numerical Value	Unit
F	Faraday's Constant	9.64853365×10^{4}	$\frac{C}{mol}$
R	Gas Constant	8.3144621	$\frac{J}{mol\,K}$
T	Temperature	2.9515×10^{2}	K
E_B	Bulk Potential	0.510	V
D	Diffusivity	1.357×10^{-5}	$\frac{cm^2}{s}$
k	Mass Transport Coefficient	1.0×10^{-2}	$\frac{cm}{s}$
MW	Molecular Weight of 316 SS	55.85	$\frac{g}{mol}$
ρ	Density of 316 SS	7.92	$\frac{g}{cm^3}$
i_A	Anodic Current Density	5.0	$\frac{A}{cm^2}$
Cl_{bulk}	Chloride Concentration in Bulk	6.00×10^{-4}	$\frac{mol}{cm^3}$
Na_{bulk}	Sodium Concentration in Bulk	5.80×10^{-4}	$\frac{mol}{cm^3}$
C_{bulk}	Metal Concentration in Bulk	1.00×10^{-5}	$\frac{mol}{cm^3}$
C_{solid}	Metal Concentration at Solid Interface	0.143	$\frac{mol}{cm^3}$
C_{sat}	Concentration of Metal at Saturation Limit	5.18×10^{-3}	$\frac{mol}{cm^3}$
γ	Saturation Multiplier	0.6	N/A

3.2 Stage II Implementation

Equation (2.41) is implemented numerically by using a forward Euler's method at each time step. The derivative $\frac{\partial h}{\partial t}$ is approximated by

$$\frac{\partial h}{\partial t} \approx \frac{h^{(n+1)} - h^{(n)}}{dt}, \tag{3.4}$$

so (2.45) can then be written as

$$h^{(n+1)} = h^{(n)} + dt\frac{D}{C_{solid} - \gamma C_{sat}}\left(\frac{\partial C}{\partial z}\right)_N, \tag{3.5}$$

where $\left(\frac{\partial C}{\partial z}\right)_N$ is the value of the derivative at the pit bottom. Note that the time evolution of the potential (and thus also the concentration) at time step n depends upon the total damage at time step n. Therefore, to make sense of (3.5) we must evaluate the derivative at the previous time step. By using $z = h^{(n)}$ in (2.44), equation (3.5) is then simplified to

$$h^{(n+1)} = h^{(n)} + dt\frac{D}{C_{solid} - \gamma C_{sat}}\left(\frac{\gamma C_{sat} - C_{bulk}}{h^{(n)}}\right). \tag{3.6}$$

When we equate (2.45) with (2.6), we have

$$\frac{D}{C_{solid} - \gamma C_{sat}}\left(\frac{\gamma C_{sat} - C_{bulk}}{h^{(n)}}\right) = \frac{i_A MW}{2\rho F}. \tag{3.7}$$

This shows that the required damage in order to reach a specified current density i_A by the end of Stage II is given by

$$h = \frac{2\rho F D}{C_{solid} - \gamma C_{sat}}\left(\frac{\gamma C_{sat} - C_{bulk}}{i_A MW}\right). \tag{3.8}$$

Additionally, the diffusion limited current density can be plotted against the inverse pit depth according to

$$i_L = \frac{2\rho FD}{C_{solid} - \gamma C_{sat}} \left(\frac{\gamma C_{sat} - C_{bulk}}{MW} \right) \frac{1}{h}. \tag{3.9}$$

Equation (3.9) shows i_L is inversely proportional to pit depth z where the proportionality constant is

$$m = \frac{2\rho FD}{C_{solid} - \gamma C_{sat}} \left(\frac{\gamma C_{sat} - C_{bulk}}{MW} \right), \tag{3.10}$$

which is an analytic expression for the slope. By using separation of variables on (2.45) we obtain

$$h^2 = \frac{2D(\gamma C_{sat} - C_{bulk})}{C_{solid} - \gamma C_{sat}} t, \tag{3.11}$$

which can be inverted to give us

$$\frac{1}{h^2} = \frac{C_{solid} - \gamma C_{sat}}{2D(\gamma C_{sat} - C_{bulk})} \frac{1}{t}. \tag{3.12}$$

Then by squaring both sides of (3.9) and using (3.12), we obtain an expression for i_L^2 in terms of $\frac{1}{t}$,

$$i_L^2 = \frac{2D(\rho F)^2}{(C_{solid} - \gamma C_{sat})} \frac{(\gamma C_{sat} - C_{bulk})}{MW^2} \frac{1}{t}. \tag{3.13}$$

We simplify by using $C_{solid} = \dfrac{\rho}{MW}$:

$$i_L^2 = \frac{2D(FC_{solid})^2(\gamma C_{sat} - C_{bulk})}{C_{solid} - \gamma C_{sat}} \left(\frac{1}{t}\right). \tag{3.14}$$

Thus, if i_L^2 is plotted against $\dfrac{1}{t}$ the slope of the graph is given by

$$m = \frac{2D(FC_{solid})^2(\gamma C_{sat} - C_{bulk})}{C_{solid} - \gamma C_{sat}}. \tag{3.15}$$

The analytic expressions (3.10) and (3.15) are compared against experimental data in our results in Chapter 4. At the start of Stage II, we begin the iteration process to determine the damage in (3.6) by using the value of the derivative at the end of Stage I. We use our initial calculation for the damage to determine an initial potential curve by solving (2.30) subject to conditions (2.33) and (2.37). Prior to stepping down the potential, we hold the potential fixed and we update the damage and concentration profiles in time until we have reached the desired pit depth. We then linearly step down the bulk potential by using the scan rate of 5 mV/s to be consistent with the experiment by Srinivasan et al. [16]. Again, the damage and concentration profiles are updated at each time step. We use the number of time steps required for the potential E_N to be stepped down to the transition value $E_N = E_T \approx 0.025\,V$.

The following is a step by step implementation for the Stage II model:

1. Determine the value of the potential at the bottom of the pit $E(z = h)$ in (2.37).

2. Use the value of $\frac{\partial C}{\partial z}$ from the previous time step to update the damage using Euler's Method in (3.6) and to update the z grid.

3. Use the new z grid to determine the potential $E(z)$ by solving equation (2.30) at the previous time step (the transition time at the end of Stage I) subject to the boundary conditions (2.33) and (2.37).

4. Determine the concentrations of sodium, chloride and metal ions by using the analytic expression in (2.43). Determine the derivative $\frac{\partial C}{\partial z}$ using (2.44). The critical values of sodium and chloride concentrations are found as Cl_N^- and Na_N^+ from the end of Stage I.

5. While holding the potential E fixed, update the damage at time step n for $h^{(n+1)}$ and the z grid by using Euler's Method in (3.6) with increment dt. Use the new value of h and the new z grid to update each of the concentration profiles.

6. Exit the time loop when the desired pit depth is reached.

7. Enter a new time loop. For time step n, linearly decrease the bulk value of the potential using the scan rate of 5 mV/s and repeat steps (1) - (4).

8. Exit the time loop after the potential at the bottom of the pit E_N has been stepped down to the transition value $E_N = E_T \approx 0.025V$.

9. Determine the limiting current density by using the damage profile in equation (3.9).

A list of the parameters used in Stage II of the model is given in Table 3.2. The values for E_T and i_T are chosen to match the data in Srinivasan et al. [16].

Table 3.2: Stage II Model Parameters (Baseline)

Variable Name	Description	Numerical Value	Unit
F	Faraday's Constant	9.64853365×10^{4}	$\frac{C}{mol}$
R	Gas Constant	8.3144621	$\frac{J}{mol\,K}$
T	Temperature	2.9815×10^{2}	K
E_B	Bulk Potential	0.510	V
E_T	Transition Potential (target)	0.025	V
i_T	Transition Current Density (target)	0.50	$\frac{A}{cm^2}$
D	Diffusivity	1.357×10^{-5}	$\frac{cm^2}{s}$
MW	Molecular Weight of 316 SS	55.85	$\frac{g}{mol}$
ρ	Density of 316 SS	7.92	$\frac{g}{cm^3}$
Cl_{bulk}	Chloride Concentration in Bulk	6.0×10^{-4}	$\frac{mol}{cm^3}$
Na_{bulk}	Sodium Concentration in Bulk	5.8×10^{-4}	$\frac{mol}{cm^3}$
C_{bulk}	Metal Concentration in Bulk	1.0×10^{-5}	$\frac{mol}{cm^3}$
C_{solid}	Metal Concentration at Solid Interface	0.143	$\frac{mol}{cm^3}$
C_{sat}	Concentration of Metal at Saturation Limit	5.18×10^{-3}	$\frac{mol}{cm^3}$
γ	Saturation Multiplier	0.6	N/A

3.3 Stage III Implementation

The damage h in Stage III is very similar to (3.2), only the current density i_A is no longer a constant but varies as a function of potential, so we must use Euler's method. The damage equation is then

$$h^{(n+1)} = h^{(n)} + dt\frac{i_A(E_N)\,MW}{2\rho F}, \tag{3.16}$$

where $i_A(E_N)$ is the current density evaluated at the potential value E_N. The current density is evaluated using the polarization curve for Stage III in Figure 1.1. We implement an artificial curve fit through the two points (i_{RP}, E_{RP}) and (i_T, E_T) where the potential is an exponential function of the current

$$E = \theta + \eta e^{\zeta i_A}. \tag{3.17}$$

Or as an expression for the current as a function of potential

$$i_A(E) = \frac{1}{\zeta} log\left(\frac{E-\theta}{\eta}\right). \tag{3.18}$$

We have chosen ζ to be a free parameter to control the slope of the exponential curve while the values of θ and η are determined using the two interpolating points as follows

$$\theta = \frac{\left(e^{\zeta i_{RP}}\right)E_T - \left(e^{\zeta i_T}\right)E_{RP}}{e^{\zeta i_{RP}} - e^{\zeta i_T}}, \tag{3.19}$$

$$\eta = \frac{E_{RP} - \theta}{e^{\zeta i_{RP}}}. \tag{3.20}$$

The repassivation values we take from Table 1.1 to be $E_{RP} = -0.16V$ and $i_{RP} = 3.0 \times 10^{-5} \frac{A}{cm^2}$. The limiting transition values of E_T and i_T are taken as the potential and current density at the bottom of the pit for the final time step in Stage II. In order to determine the potential in Stage III, we simulate the approach to repassivation when the metal oxide layer fully forms and the pit shuts down by stepping down the value of E_B. We take E_B at the start of Stage III to be the value E_1 at the end of Stage II. We begin the iteration in (3.16) by evaluating the current density in (3.18) using the potential $E_N = E_T$. The current density and damage are then used to solve equation (2.30) subject to the conditions (2.48) and (2.49) in order to determine the potential. The time loop is created by using the previous value E_N to update the current in (3.18) and the damage in (3.16). At each iteration, the value of E_B is stepped down using the chosen scan rate. We stop Stage III when the potential at the bottom of the pit reaches the repassivation value $E_N = E_{RP} \approx -0.16V$. The following is a step by step implementation for the Stage III model:

1. Choose a value of the free parameter ζ. Use the final values of potential and current from the end of Stage II as the transition values of potential E_T and current i_T. Use $i_{RP} = 3.0 \times 10^{-5} \frac{A}{cm^2}$ and $E_{RP} = E_T - 0.185V$ as estimates for the repassivation values. Determine θ and η using (3.19) and (3.20) and use the fitting parameters to determine the polarization curve defined in (3.18).

2. Use the polarization curve and the previous potential E_N to determine the current density $i_A(E_N)$. Use it to update the damage using Euler's Method in (3.16) with increment dt and to update the z grid.

3. Use the new z grid to determine the potential $E(z)$ by solving equation (2.30) subject to the boundary conditions (2.48) and (2.49).

4. Determine the concentrations of sodium, chloride, and metal ions by using the potential in the electroneutraility condition (2.22).

5. For time step n, linearly decrease the bulk potential using the scan rate of $5\,mV/s$ and repeat steps (2)-(4).

6. Exit the time loop after the potential at the bottom of the pit E_N has been stepped down to the repassivation value $E_N = E_{RP} \approx -0.16\,V$.

A list of the parameters used in Stage III of the model is given in Table 3.3. The values for E_{RP} and i_{RP} are chosen to match the data in Srinivasan et al. [16]. The parameter ζ is chosen so that the current $i_A(E)$ has a moderately steep slope.

Table 3.3: Stage III Model Parameters (Baseline)

Variable Name	Description	Numerical Value	Unit
F	Faraday's Constant	9.64853365×10^{4}	$\frac{C}{mol}$
R	Gas Constant	8.3144621	$\frac{J}{mol\,K}$
T	Temperature	2.9815×10^{2}	K
E_B	Bulk Potential	0.510	V
E_{RP}	Repassivation Potential (Target)	-0.16	V
D	Diffusivity	1.357×10^{-5}	$\frac{cm^2}{s}$
MW	Molecular Weight of 316 SS	55.85	$\frac{g}{mol}$
ρ	Density of 316 SS	7.92	$\frac{g}{cm^3}$
i_{RP}	Repassivation Current Density (Target)	3.0×10^{-5}	$\frac{A}{cm^2}$
Cl_{bulk}	Chloride Concentration in Bulk	6.0×10^{-4}	$\frac{mol}{cm^3}$
Na_{bulk}	Sodium Concentration in Bulk	5.8×10^{-4}	$\frac{mol}{cm^3}$
C_{bulk}	Metal Concentration in Bulk	1.0×10^{-5}	$\frac{mol}{cm^3}$
C_{solid}	Metal Concentration at Solid Interface	0.143	$\frac{mol}{cm^3}$
C_{sat}	Concentration of Metal at Saturation Limit	5.18×10^{-3}	$\frac{mol}{cm^3}$
γ	Saturation Multiplier	0.6	N/A
ζ	Free Parameter for Polarization Curve	10	N/A

CHAPTER IV

RESULTS AND DISCUSSION

4.1 Results

In the Stage I model, we solve equation (2.30) subject to the boundary conditions (2.31) and (2.32) in MATLAB by using the ode45 solver. We use $h^{(1)} = 1.0\ \mu m$ for an initial value of the damage and time increment $dt = 0.1$ seconds to update the damage profile according to (3.2). After determining the potential E at a given time step, we then calculate the concentration of iron ions C as well as the concentrations of sodium and chloride by using the electroneutrality condition (2.22). We choose the bulk iron and bulk chloride concentrations to be $C_{bulk} = 1.0 \times 10^{-5}\ \frac{mol}{cm^3}$ and $Cl_{bulk} = 6.0 \times 10^{-4}\ \frac{mol}{cm^3}$, and the bulk sodium concentration is obtained from electroneutrality. The simulation is run for a total of 17.8 seconds, which is the length of time required for the concentration to reach 60 % of the saturation value $C_{sat} = 5.18 \times 10^{-3} \frac{mol}{cm^3}$. Plots of E, C, and concentrations of sodium and chloride all versus pit depth z are given in Figures 4.1 through 4.8. Figures 4.1 through 4.4 show early time growth and are plotted for the first 0.3 seconds of the simulation. Note that each time step corresponds to a plot with varying length. Because a viewing window could not be chosen so that individual time steps could be distinguished while the damage at the

end of each time step was also clearly visible, we label the damage for each time step to clarify the fact that the pit continues growing past the edge of the viewing window. Note that our chosen viewing window was only able to display a small fraction of the total damage in each time step, as evident of the fact that the largest value on our x-axis is $0.01\,\mu m$ Figures 4.5 through 4.8 are plotted over the entire length of Stage I, and the output is displayed after every 4 time steps ($0.4\ s$). Note that the y-axis changes slowly in time, which causes each new plot that is displayed to have substantial overlap with the previous one. To show the progression of the system over time, the damage is labeled after 4 s, 8 s, 12 s, 16 s and 17.8 s.

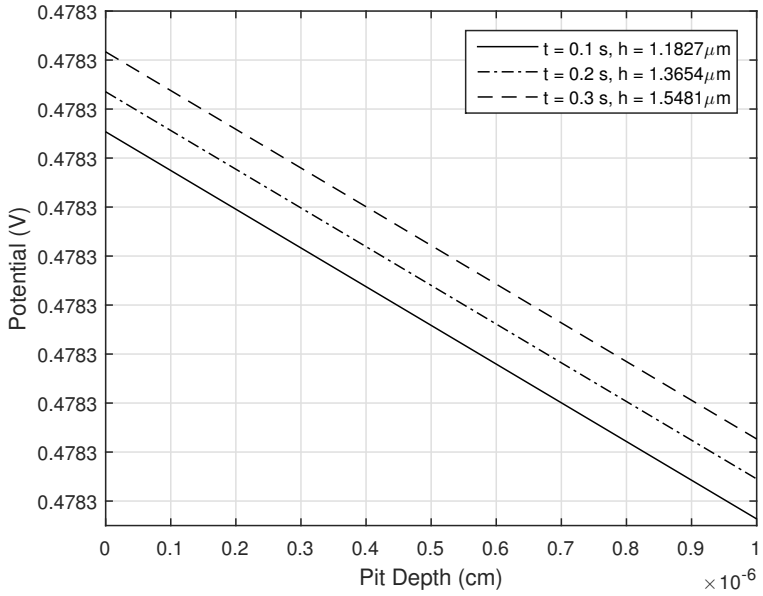

Figure 4.1: Potential E vs pit depth z for Stage I shown for the first 0.3 seconds of growth.

It is clear from Figure 4.5 that the effective potential at $z = 0$ is less than the bulk value $E_B = 0.510\,V$. This is because the semi-permeable membrane acts as

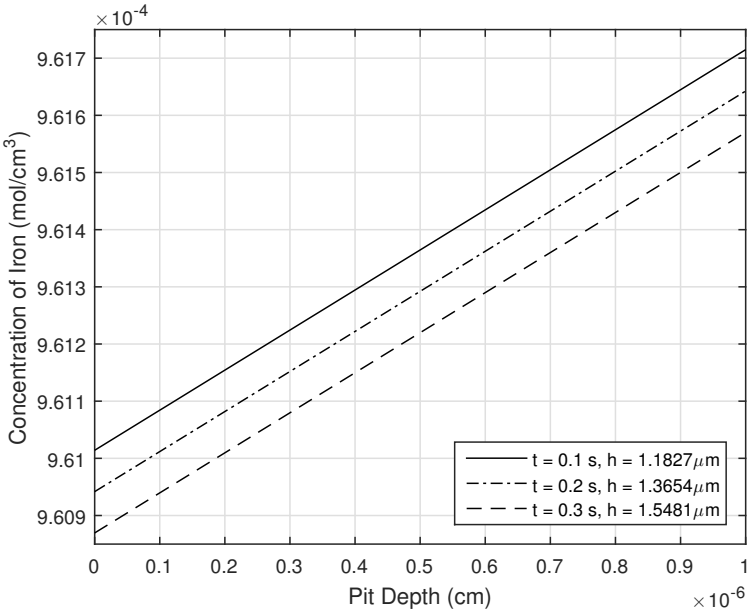

Figure 4.2: Iron concentration C vs pit depth z for Stage I shown for the first 0.3 seconds of growth.

a resistive layer and slows down the flow of the metal ions at the pit cover. Another observation is that the potential at the pit cover increases slightly in time. According to Frankel et al. [15], the resistance of a porous pit cover for hemispherical pits was found to decrease with the inverse square of pit depth. Additionally, as we discussed in Chapter 1, because the current for hemispherical pits increases with the square of the radius, the IR drop was found to be approximately constant, leading to a constant current density. Therefore, our observed result that the potential at the pit mouth increases in time is inconsistent with a constant IR drop, because our potential at the pit bottom is shown to decrease in time.

We report the minimum value of the potential at the end of Stage I to be 0.450284 V, which is very close to the target value of the potential that we use

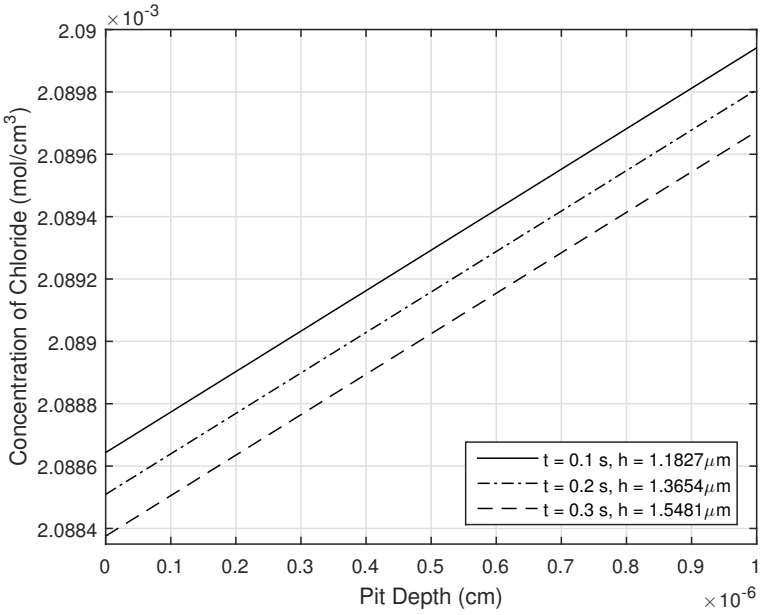

Figure 4.3: Chloride concentration $[Cl^-]$ vs pit depth z for Stage I shown for the first 0.3 seconds of growth.

for the potentiostatic hold at the beginning of Stage II, which is $E_{Hold} = 0.45\,V$ as presented on the polarization curve. We also note that the potential appears to decrease exponentially, but the slope is shallow enough that the graph appears nearly linear.

As seen in Figure 4.2, i.e., the concentration of iron at the pit cover decreases slightly in time, and in Figure 4.6 the concentration at the bottom of the pit increases in time until it reaches the critical saturation level $\gamma C_{sat} = 3.108 \times 10^{-3}\,\frac{mol}{cm^3}$. This buildup of iron at the surface of the interface is due to the fact that the dissolution rate of the metal is faster than the diffusion rate. We also note that the concentration increases linearly with pit depth.

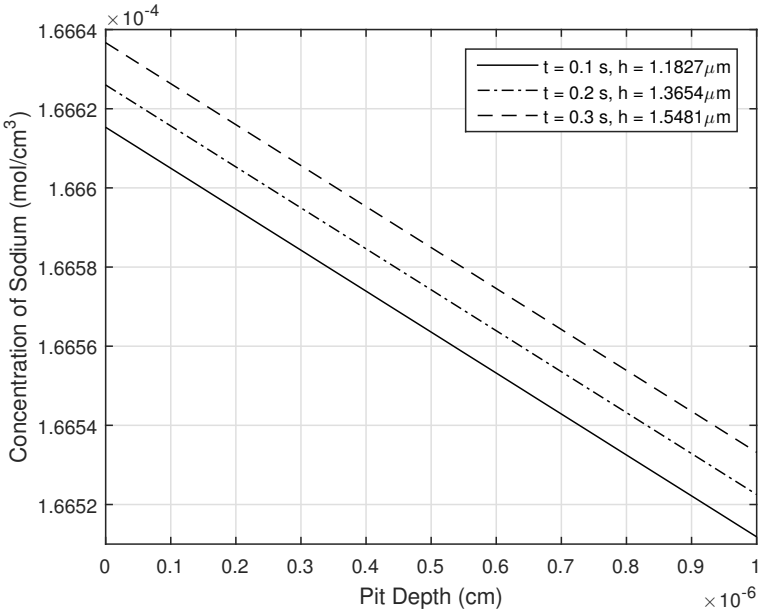

Figure 4.4: Sodium concentration $[Na^+]$ vs pit depth z for Stage I shown for the first 0.3 seconds of growth.

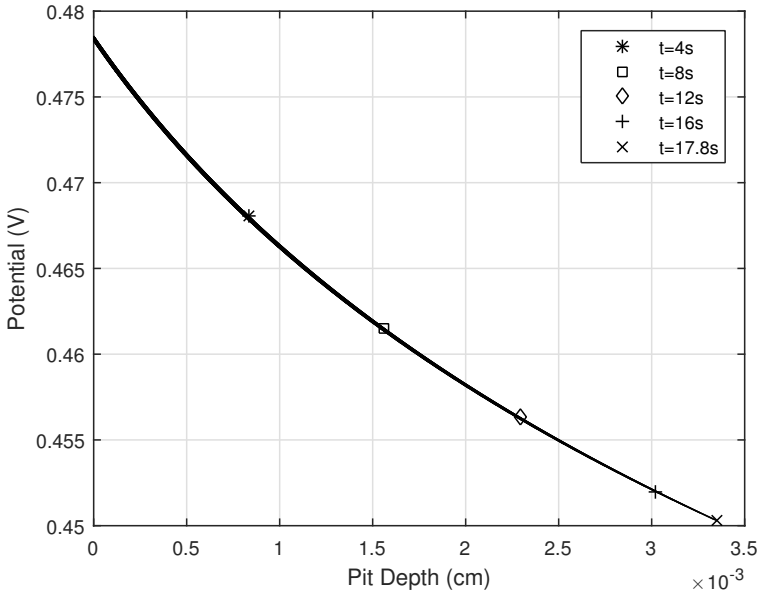

Figure 4.5: Potential E vs pit depth z for Stage I.

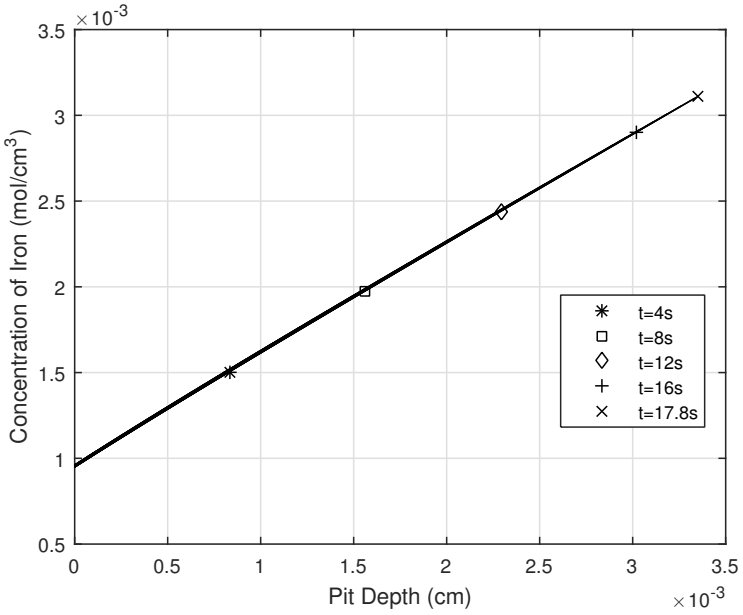

Figure 4.6: Iron concentration C vs pit depth z for Stage I.

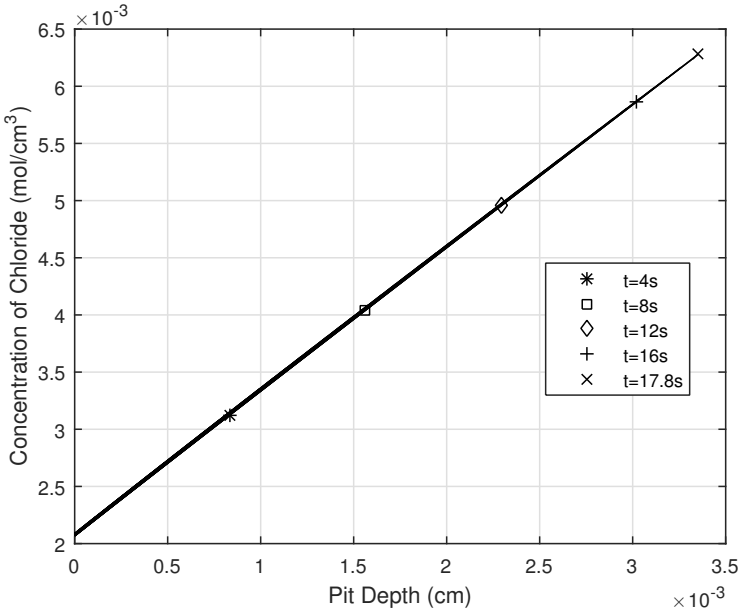

Figure 4.7: Chloride concentration $[Cl^-]$ vs pit depth z for Stage I.

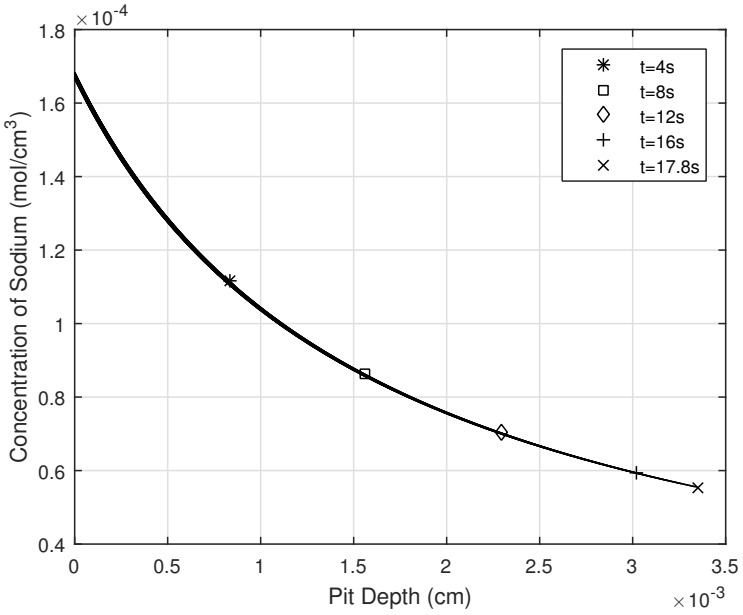

Figure 4.8: Sodium concentration $[Na^+]$ vs pit depth z for Stage I.

In Figures 4.3 and 4.7, we see that the chloride concentration follows the same trend as the iron in Figures 4.2 and 4.6: the concentration increases as the pit depth increases. This is because the chloride ions enter the pit in order to maintain electroneutrality within the pit. In Figures 4.4 and 4.8, the sodium concentration follows an inverse trend to the chloride, also in accordance to electroneutrality. Because the iron concentration increases as pit depth increases, the sodium concentration decreases as pit depth increases because both ions are positively charged. It is reasonable that both the concentrations of iron and chloride are linear because the sodium concentration has a small magnitude and thus its exponential shape has little effect on the shape of the iron concentration.

A graph of pit depth z versus total time elapsed for Stage I is shown in Figure 4.9. The graph is linear, which is consistent with i_A being constant, so that $\frac{\partial h}{\partial t}$ is constant. The total damage h at the end of Stage I is $33.52\,\mu m$.

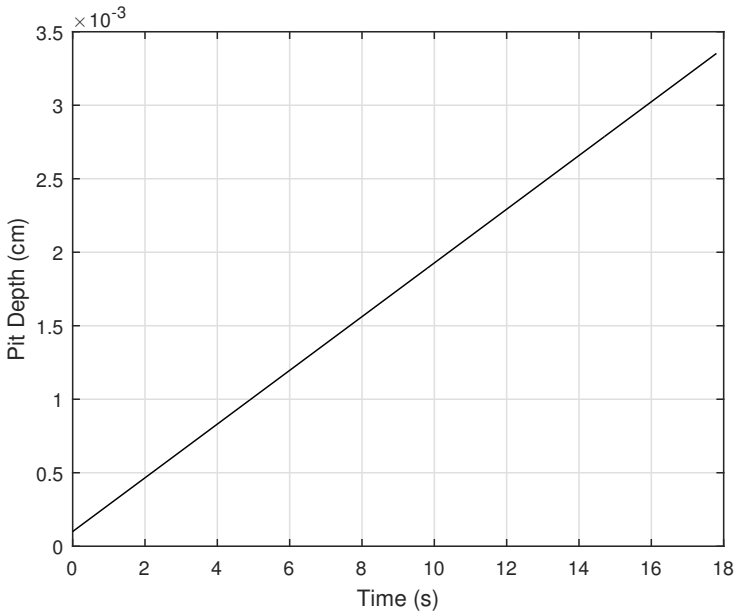

Figure 4.9: Pit depth z vs time elapsed t for Stage I.

In the Stage II model, (2.30) is solved subject to the boundary conditions (2.33) and (2.37). Initially, the potential is held fixed as we update the total damage in time using time increment $dt = 5$ seconds according to (2.45). The potential was held for a total of 310 seconds until the pit reached a depth of 141.93 μm. This time period is chosen to match the long potentiostatic hold at 0.45 V in Srinivasan et al. [16] (Figure 3a [16]) and to generate significant pit growth. At each time step we determine the concentrations of iron, sodium, and chloride by using the updated damage h in (2.43). Results from Stage I are shown as a solid line while the Stage

II results are shown as the "dot-dash" pattern. The potential E is plotted against the pit depth z for the potentiostatic hold in Figure 4.10. Results are displayed after every 6 time steps (30 s) during this portion of Stage II.

In Figure 4.10, we see that during the time that the potential is held fixed, the value of E at the pit mouth does not change from the bulk value $E_B = 0.510\,V$ because the cover is no longer there. The potential value at the pit bottom E_{hold} matches the minimum value of the potential at the end of Stage I, which is $E = 0.450284\,V$. Note that the change in potential ΔE across the pit, the potential drop, remains constant at the value $\Delta E = 0.05923\,V$ as determined by (2.38). This result is consistent with the result of Laycock [4] that the potential drop is constant in the diffusion controlled regime.

Next, we lower the bulk potential using a scan rate of $5\ mV/s$ for a total of 85.1 seconds until E reaches the transition value $E_T = 0.0252\,V$. Because the potential drop in (2.38) is not a function of the bulk potential, we have $\Delta E = 0.05923\,V$ as E_B is decreased during the scanning process. Therefore, when we lower the bulk value, the potential curve is uniformly lowered by the same amount. Using $dt = 0.1$ seconds we update the total damage in time according to (2.45) and update the concentration profiles using electroneutrality. The total damage at the end of Stage II is 159.07 μm, which is the depth required for our diffusion limited current density to reach $i_T = 0.5214\,\frac{A}{cm^2}$. This is fairly close to our target value of $0.50\,\frac{A}{cm^2}$. At the end of the scanning procedure, the bulk value has become $E_B = 0.0845\,V$ and the value at the pit bottom has reached $0.0252\,V$, which is very close to the target value of the transition

potential $E_T = 0.025\,V$ as presented on the polarization curve. In Figure 4.11, the potential E is plotted against pit depth z during the linear polarization scan. Results are displayed after every 50 time steps (5 s).

In Figure 4.12, we display Figures 4.10 and 4.11 together on one plot to show the overall behavior of the potential during stage II. Note that the potential in Stage II decreases exponentially much like in Stage I, but has a steeper slope than before so the graph is no longer close to being linear. We also note that almost all of the pit growth occurs during the potentiostatic hold.

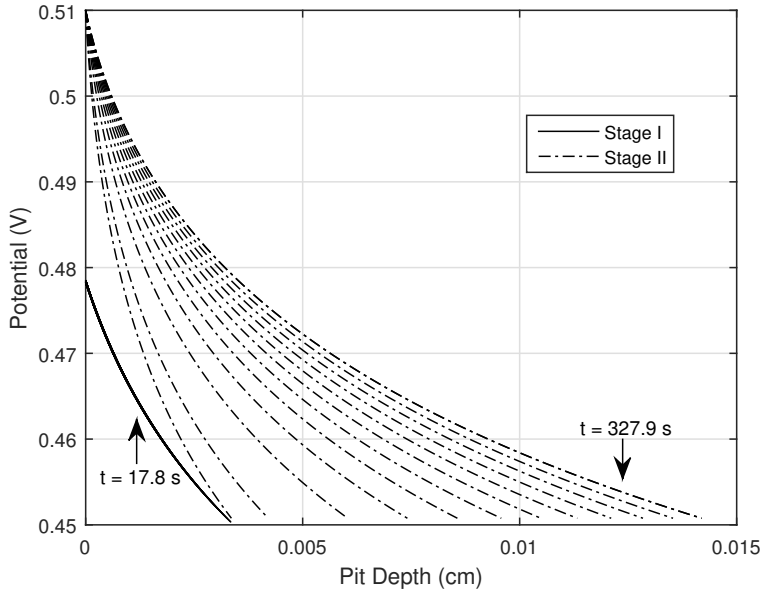

Figure 4.10: Potential E versus pit depth z during the portion of Stage II where E_B was held fixed.

A plot of the iron concentration C, and concentrations of sodium and chloride through the end of Stage II, are shown in Figures 4.13, 4.14, and 4.15.

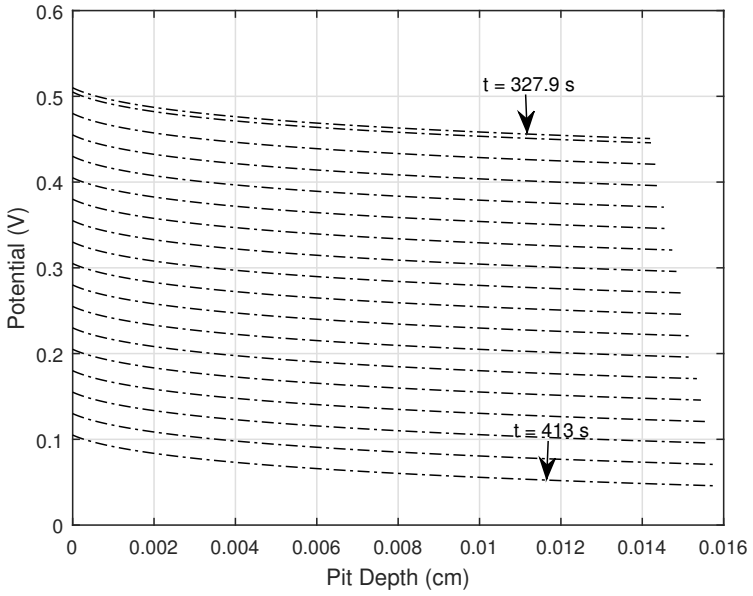

Figure 4.11: Potential E versus pit depth z during the portion of Stage II where the potential is scanned by decreasing E_B.

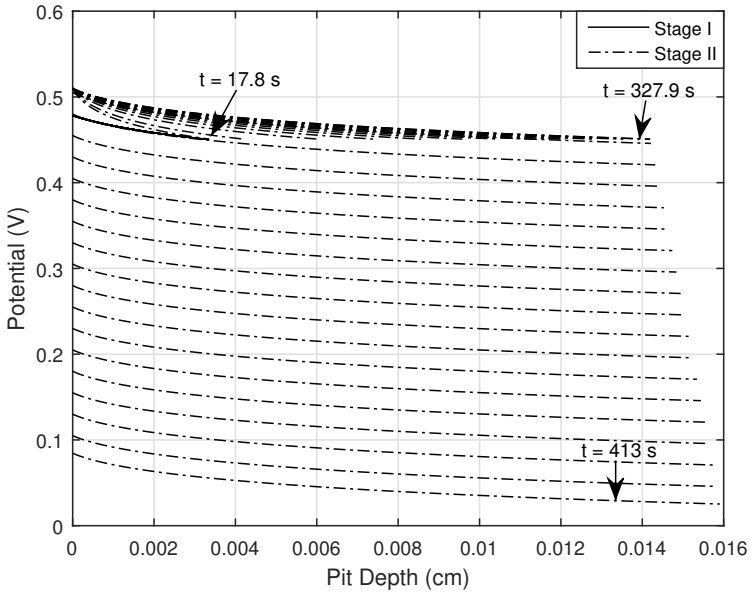

Figure 4.12: Potential E versus pit depth z through the end of Stage II.

In Figure 4.13, we note that the concentration of iron at the pit mouth remains small throughout Stage II because the pit cover is no longer present at the mouth so there is no longer a resistive layer to slow down passage of the ions. As expected, the concentration profile is linear and the value at the bottom of the pit remains at 60% of C_{sat}, which matches the concentration level at the end of Stage I. The slope of the graph decreases as the pit grows deeper. Note however, that the concentration at the pit mouth shows a sudden decrease at the beginning of Stage II. This decrease can be explained by the fact that our model is not able to account for rapid transitions in time. When we assumed the system was in steady state, we neglected the time derivative in our asymptotic expansion which was a term of $O(\epsilon)$. Therefore, we do not account for any boundary layers in time. A rapid transition in time occurs in the system between the end of Stage I and the beginning of Stage II due to the competition between the dissolution rate and the diffusion rate. In Stage I, the dissolution rate is faster than the diffusion rate accounting for the buildup of iron at the interface. In Stage II, the two rates are balanced because the system is under diffusion control. Therefore, when we rapidly transition from Stage I to Stage II in our model, we cross a boundary layer in time which leads to our sudden decrease in concentration at the pit mouth. This is consistent with our neglect of transient behavior in the potential when we assumed that the pit cover bursts instantaneously between Stages I and II, and explains the sudden increase in the potential at the pit mouth as seen in Figure 4.12. Note that a sudden change in concentration at the pit mouth due to

the boundary layer is also seen in our plots of chloride and sodium in Figures 4.14 and 4.15.

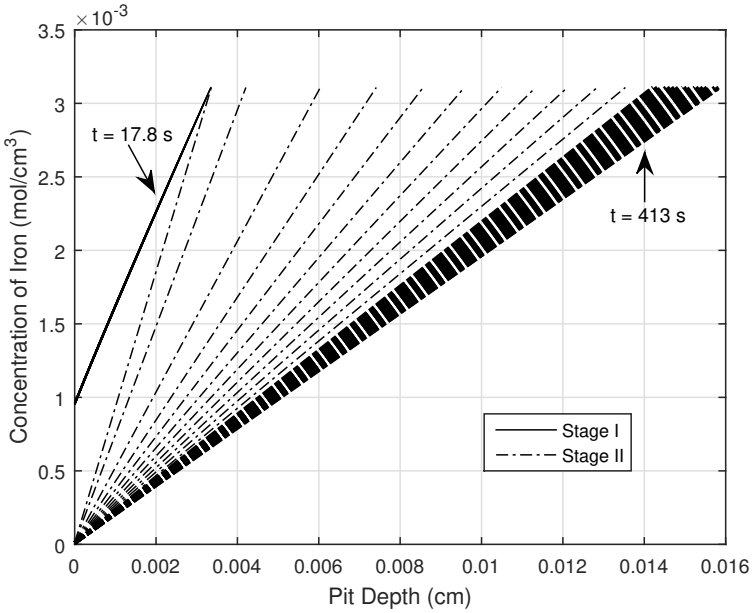

Figure 4.13: Iron concentration C versus pit depth z through the end of Stage II.

In Figure 4.14 the chloride concentration follows the exact shape of the iron concentration just as in Stage I. We also note that the change in chloride level from the mouth to the pit bottom in Stage I is roughly $4.2 \times 10^{-3} \frac{mol}{cm^3}$ which is smaller in comparison to the change of $5.7 \times 10^{-3} \frac{mol}{cm^3}$ in Stage II.

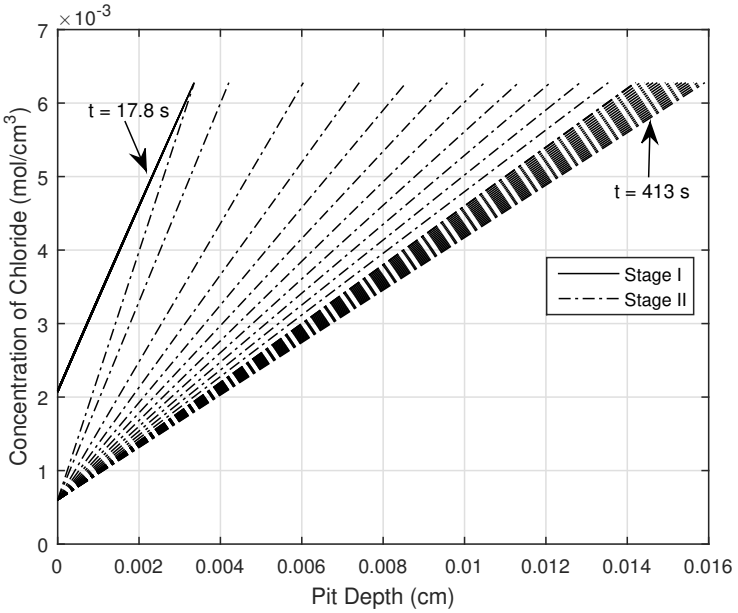

Figure 4.14: Chloride concentration $[Cl^{-}]$ versus pit depth z through the end of Stage II.

In Figure 4.15, the sodium concentration decreases linearly as pit depth increases as in Stage I. However, the concentration at the pit mouth is an order of magnitude larger due to the decrease in iron concentration, in accordance with electroneutrality.

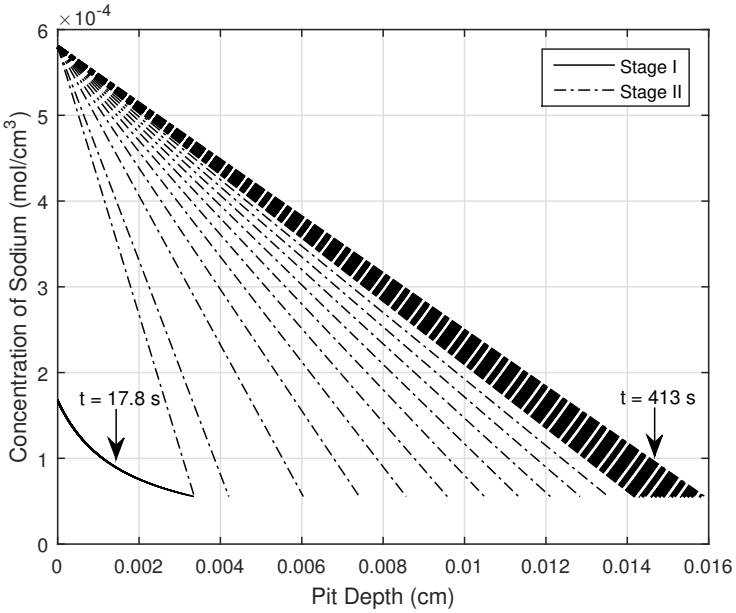

Figure 4.15: Sodium concentration $[Na^+]$ versus pit depth z through the end of Stage II.

A graph of pit depth z versus total time elapsed through the end of Stage II is shown in Figure 4.16. The damage in Stage I was curve fit with the model $h = at$ where $a = 0.0001911$, and the damage in Stage II was curve fit with the model $h = at^{1/2}$ where $a = 0.0006227$. Using (2.6) for the linear fit and (2.45) for the power fit, we calculated the respective values $a = 0.0001827$ and $a = 0.0007744$, which were reasonably close to our curve fit parameters. In each fit, the sum of the squares of the errors was very low (on the order of 1.0×10^{-5} or lower), which verifies the fact that the total damage h grows linearly during Stage I, and according with the square root of time during Stage II.

Srinivasan et al. [16] present a graph of diffusion limited current density versus inverse pit depth (Figure 7a [16]) where they obtain a value for the slope

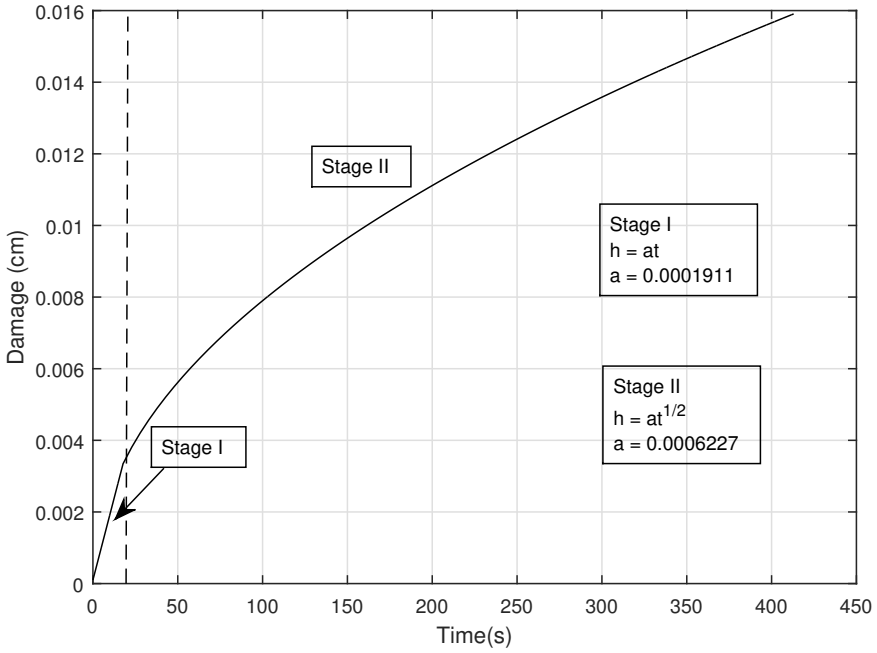

Figure 4.16: Pit depth z versus time t through the end of Stage II.

of $m = 0.830\,\frac{A}{m}$. When we choose our diffusion coefficient to be $D = 1.357 \times 10^{-5}\,\frac{cm^2}{s}$, we use (3.10) to obtain the slope $m = 0.8294\,\frac{A}{m}$, which is very close to the value stated by Srinivasan et al. Because we desire for our limiting current density at the end of Stage II to be close to $i_T = 0.50\,\frac{A}{cm^2}$, this value of D can be used in (3.8) to predict the required pit depth as $h = 165.88\,\mu m$, which we compare to the results by Srinivasan et al. [16] in a later discussion.

In Moayad et al. [13], a plot of i_L^2 versus $\dfrac{1}{t}$ is given in Figure 4 for both 316 SS and 302 SS. If we estimate their slope for 302 SS by simply eyeballing the two data points (0.001,0.15) and (0.006,0.71), we obtain the value $m = 112\,\frac{A^2 s}{cm^4}$. When we use their values $D = 1.0 \times 10^{-5}\,\frac{cm^2}{s}$, $C_{sat} = 5.866\,\frac{mol}{cm^3}$ and $\gamma = 0.62154$ in (3.15)

we obtain $m = 99.781\,\frac{A^2 s}{cm^4}$. While these two values show some discrepancy, we note that a large amount of error can be accounted for in the process of eyeballing and also in the error bars of the graph in [13]. If we use the upper error bar on the second data point assuming the value (0.006, 0.75) to recalculate the slope then we obtain $m = 120\,\frac{A^2 s}{cm^4}$, while if we use the lower error bar on the second data point assuming the value (0.006, 0.68) we obtain $m = 106\,\frac{A^2 s}{cm^4}$. These two calculated values have a 12.39% difference, supporting the fact that (3.15) is accurate as an analytic expression for the slope. We also note that (3.15) can be approximated as $m \approx 2DF^2 C_{solid}\gamma C_{sat}$ by using $\gamma C_{sat} >> C_{bulk}$ and $C_{solid} >> \gamma C_{sat}$. This is consistent with the observation in Moayad et al., that the slope is proportional to the product $D\,C_{sat}$.

By using (3.9) we are able to plot the diffusion limited current density against pit depth z in Figure 4.17. The current density decreases drastically during the period that the potential is held constant, and remains fairly constant for the remainder of Stage II when the potential is scanned. As we have already stated above, the current density at the end of Stage II was $i_T = 0.5214\,\frac{A}{cm^2}$.

In the Stage III model, equation (2.30) is solved subject to the boundary conditions (2.48) and (2.49). The current in Stage III is defined according to the polarization curve (3.18), where we choose $\zeta = 10$ and $i_{RP} = 3.0 \times 10^{-5}\frac{A}{cm^2}$. The values $i_T = 0.5214\,\frac{A}{cm^2}$ and $E_T = 0.0252\,V$ are taken from Stage II. The target value for E_{RP} is $E_{RP} = E_T - 0.185\,V = -0.1598\,V$, which is due to the 0.185 V potential difference between the target values $E_T = 0.025\,V$ and $E_{RP} = -0.160\,V$. After (2.30) is solved to determine E, the concentrations of iron, sodium, and chloride are

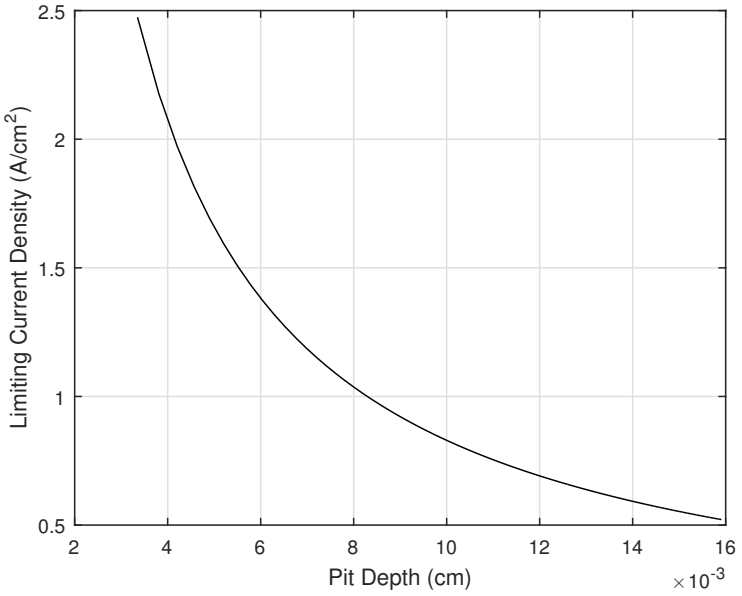

Figure 4.17: Diffusion limited current density i_L versus pit depth z.

all determined analytically using (2.43). We update the total damage using a time increment $dt = 1$ second according to (3.16). At each time step, we lower the bulk potential using a scan rate of $5\,mV/s$. The total time for Stage III was 49 seconds, which was the length of time required for the potential to reach $E_{RP} = -0.159536\,V$.

Our numerical approximation to the polarization curve is shown in Figure 4.18. Plots of E, C, and concentrations of chloride and sodium all plotted against pit depth z are shown in Figures 4.19, 4.20, 4.21, and 4.22. Results from Stage III are displayed after every 5 time steps (5 s) and are shown as dotted lines.

According to Figure 4.19, we see that the potential in Stage III continues to decay exponentially as in Stage I and II. However, the change in potential between the pit mouth and the pit bottom is not the same for each time step. Because the

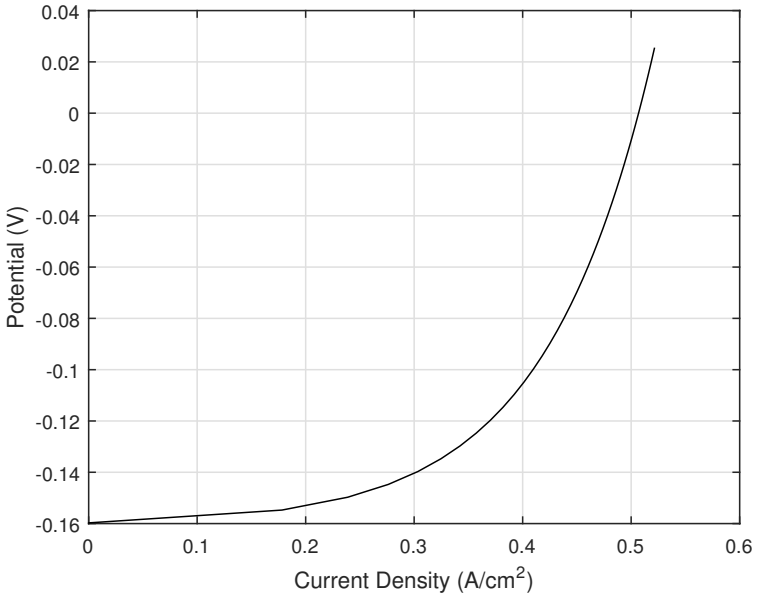

Figure 4.18: The numerical approximation to the polarization curve in Stage III.

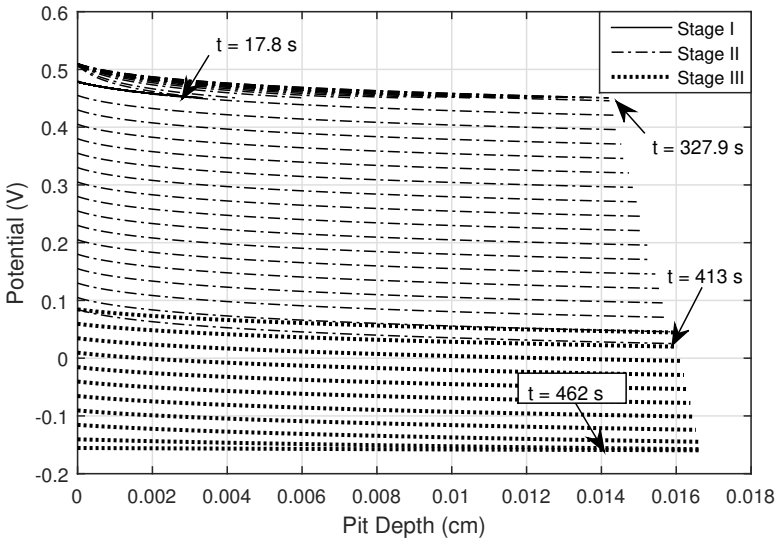

Figure 4.19: Potential E versus pit depth z through the end of Stage III.

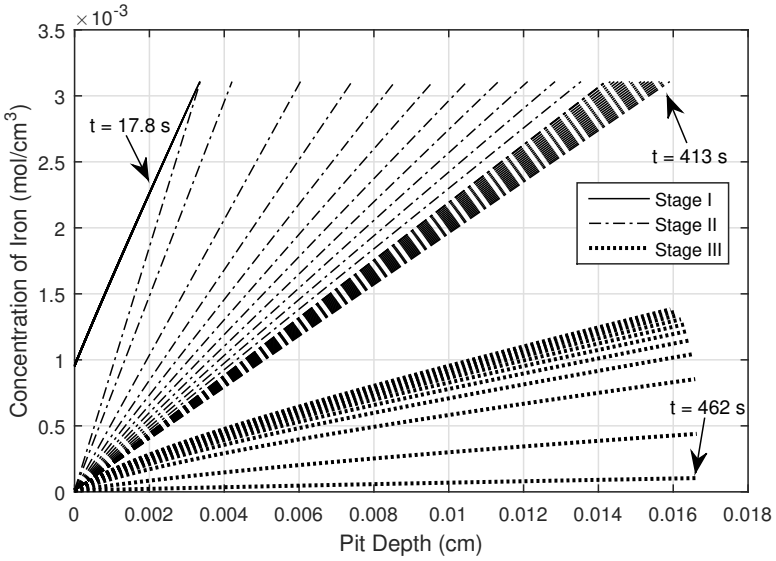

Figure 4.20: Iron concentration C versus pit depth z through the end of Stage III.

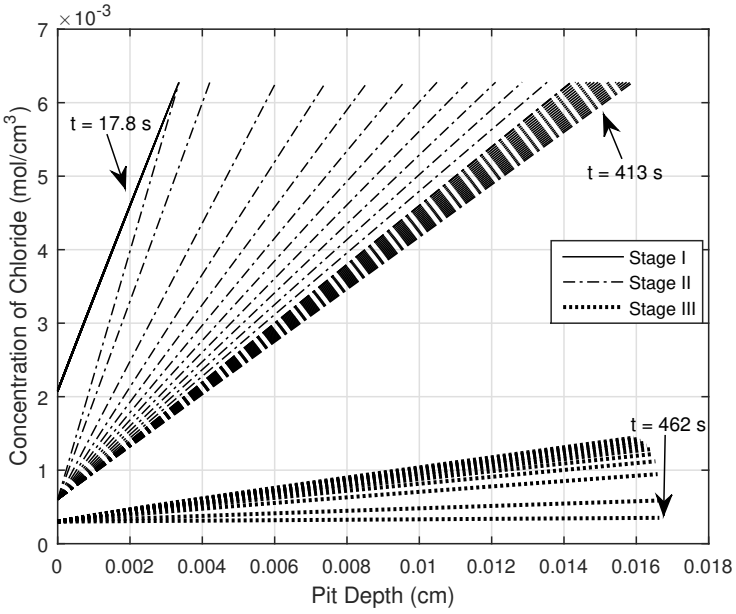

Figure 4.21: Chloride concentration $[Cl^-]$ versus pit depth z through the end of Stage III.

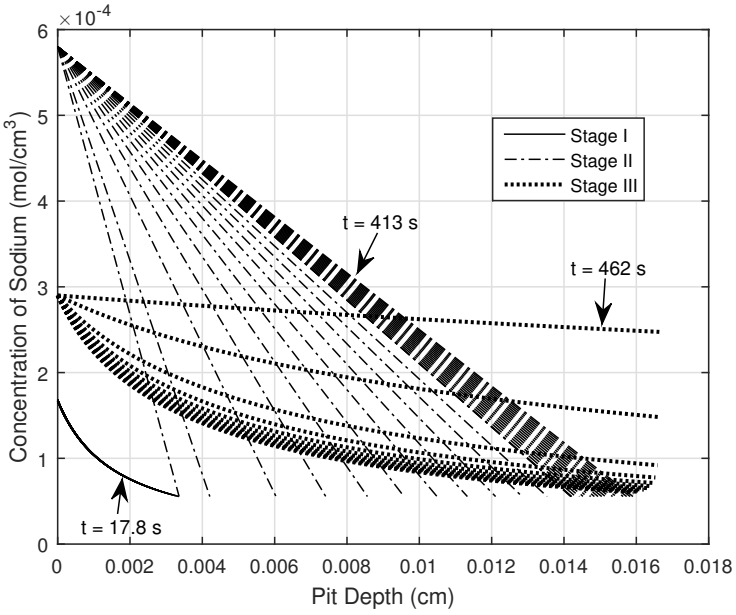

Figure 4.22: Sodium concentration $[Na^+]$ versus pit depth z through the end of Stage III.

potential at the pit bottom $E(z = h)$ depends upon the bulk value, we note that $E(z = h)$ does not decrease uniformly in time. This causes there to be a smaller change in potential from the pit mouth to the pit bottom at the end of Stage III than there is at the beginning. At the end of Stage III, we have $E(z = h) = E_{RP}$.

In Figure 4.20 we see that at the beginning of Stage III there is a sharp decrease in C at the pit bottom in comparison to the end of Stage II. At the beginning of Stage III, the diffusion rate becomes faster than the dissolution rate of the metal as the pit begins to repassivate. Thus, when we rapidly transition between the end of Stage II and the beginning of Stage III, we cross a boundary layer in time which leads to the sharp decrease in C at the pit bottom. A sudden change in concentration

at the pit bottom due to the boundary layer is also seen in our plots of chloride and sodium in Figures 4.21 and 4.22.

The concentration continues to decrease in time as the pit depth increases. This is due to the fact that as the metal repassivates and the current density drops, the available chloride that can be used in the reaction at the pit bottom (and thus also the available iron) also decreases. This is consistent with the graph of the chloride concentration in Figure 4.21.

In Figure 4.22 we see that the sodium concentration at the pit bottom in Stage III increases very quickly as pit depth increases, in order to maintain electroneutrality as the iron and chloride concentrations greatly decrease.

A plot of the pit depth z versus total time elapsed for all three stages of the model is shown in Figure 4.23, and a zoomed in plot showing only Stage III growth is shown in Figure 4.24. The total pit depth was $166.36\,\mu m$. When we compare this value to the results from Srinivasan et al. in Figure 7a [16], we see that the inverse depth at the value $i_T = 0.50\,\frac{A}{cm^2}$ is roughly $0.006\ (\mu m)^{-1} = 166.66\,\mu m$, which is close to our depth value considering that we are simply eyeballing the data point. Both of these values are close to the pit depth $h = 165.88\,\mu m$ that we predicted using (3.8).

We curve fit the damage h to the power law at^b in MATLAB using nonlinear least squares with the function fminsearch. The fit parameters for this case are $a = 0.0006358$, $b = 0.5352$. This value of b is consistent with the fact that the majority of the pit growth in the model occurs during Stage II, when the damage grows according to the square root of time. However, the power law model does

not apply to the end of Stage III because there is an asymptotic slowdown in the damage evolution as the system approaches repassivation. For the scan rate used in Figures 4.23 and 4.24, the overall deviation is slight because Stage III has a short duration. For example, truncating the data at 430 seconds (the end of the early time growth phase for Stage III) yields $b = 0.5366$, only a slight difference from the value $b = 0.5352$ obtained from using the entire data set. Figure 4.24 clearly shows that the growth is significantly slower than the power law model with $b \approx 1/2$ at the end of Stage III.

However, for a shorter scan rate, the duration of Stage III increases, so the asymptotic slowdown in the damage evolution has a more pronounced effect on the global curve fit. Therefore, it becomes more important to truncate the Stage III data at the end of the early time growth phase. For example, reducing the Stage III scan rate from $5\,mV/s$ to $0.2\,mV/s$ causes Stage III to last for a total of 1181 seconds and the total time of the simulation to last 1594 seconds. If we choose a cutoff of $t = 900\,s$, then the value of b for the fit changes from $b = 0.5558$ to $b = 0.5480$ which is a significant difference. Also note that the sum of the squares of the errors (SSE) for the fit is reduced from 1.964×10^{-4} to 4.182×10^{-5}.

A plot of the current density versus total time elapsed for all three stages of the model is shown in Figure 4.25. The current density stays constant at $i_A = 5.0\,\frac{A}{cm^2}$ for the duration of Stage I. At the beginning of Stage II, there is a sudden decrease in the current density to roughly $2.5\,\frac{A}{cm^2}$ due to the pit cover bursting. For the remainder of Stage II, the current density steadily decreases as pit depth increases

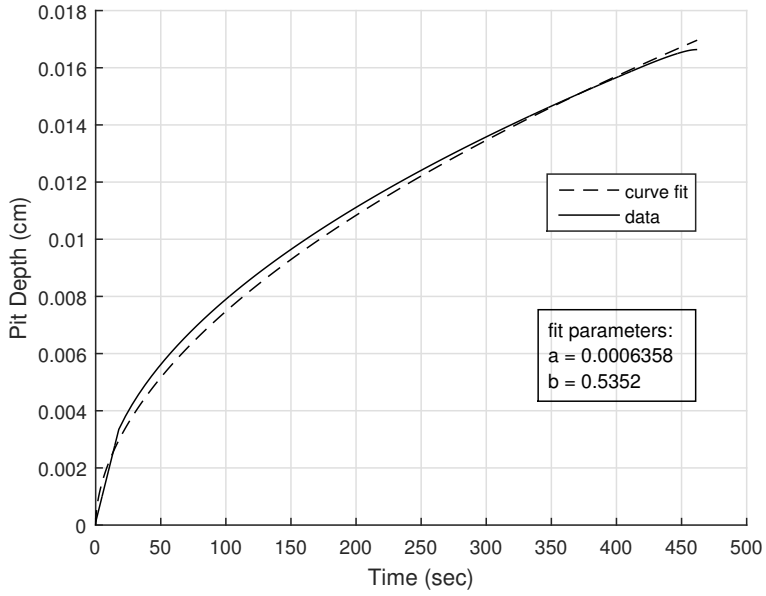

Figure 4.23: Pit depth z versus time elapsed t through the end of Stage III. The graph is curve fit by the power law $h(t) = at^b$.

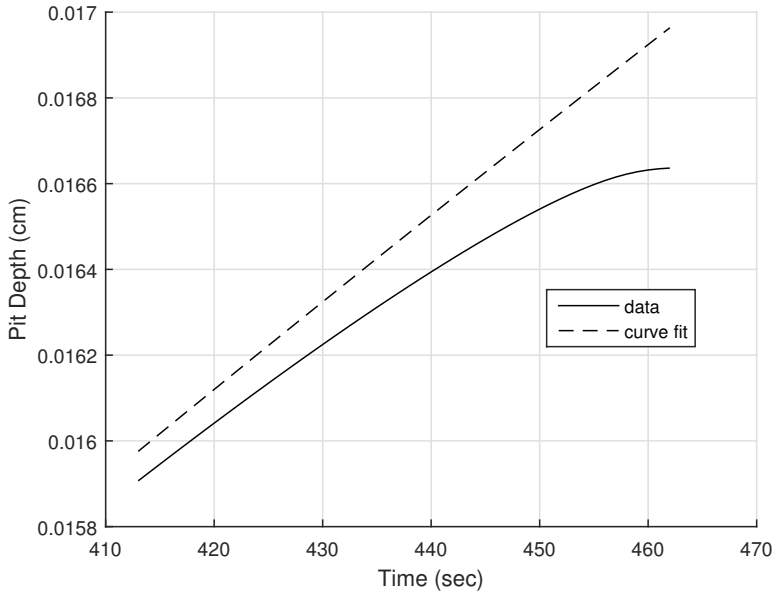

Figure 4.24: A zoomed in plot of Figure 4.23 to show Stage III growth.

according with (3.9) until it reaches $i_T = 0.5214\,\frac{A}{cm^2}$. In Stage III, the current density continues to decrease until it reaches the repassivation value $i_{RP} = 4.44 \times 10^{-2}\,\frac{A}{cm^2}$.

A plot of the chloride concentration at the metal interface versus pit depth z is shown for all three stages in Figure 4.26. We see that the chloride at the interface grows steadily throughout Stage I due to the increase in pit depth and iron concentration due to dissolution, and then remains constant at saturation throughout Stage II. Following a sharp decline, the chloride steadily decreases throughout Stage III as the metal repassivates. This sharp decline is consistent with the decline as shown in Figure 4.21 due to the fact that transient behavior is neglected between Stages II and III. We note that this is the same general trend that is displayed in Mankowski et al. [21] in their plot of chloride concentration versus pit diamater (Figure 1 [21]), with the exception that Mankowski does not show a sharp decline prior to repassivation.

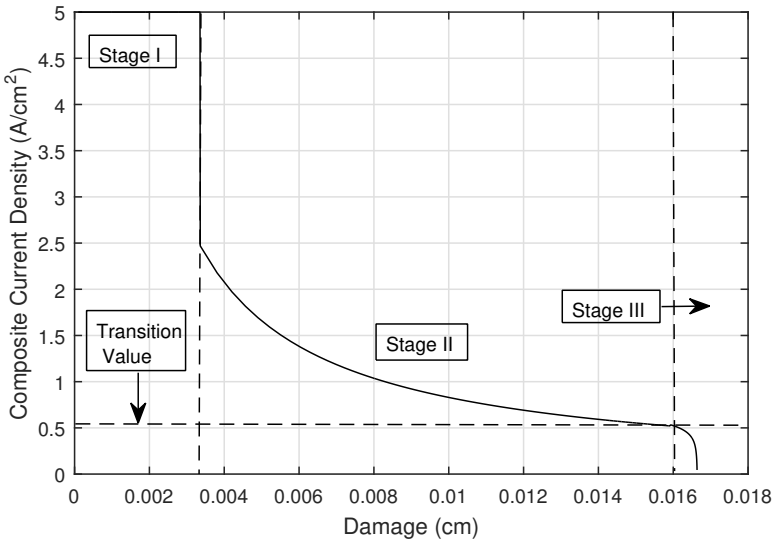

Figure 4.25: Current density versus pit depth z through the end of Stage III.

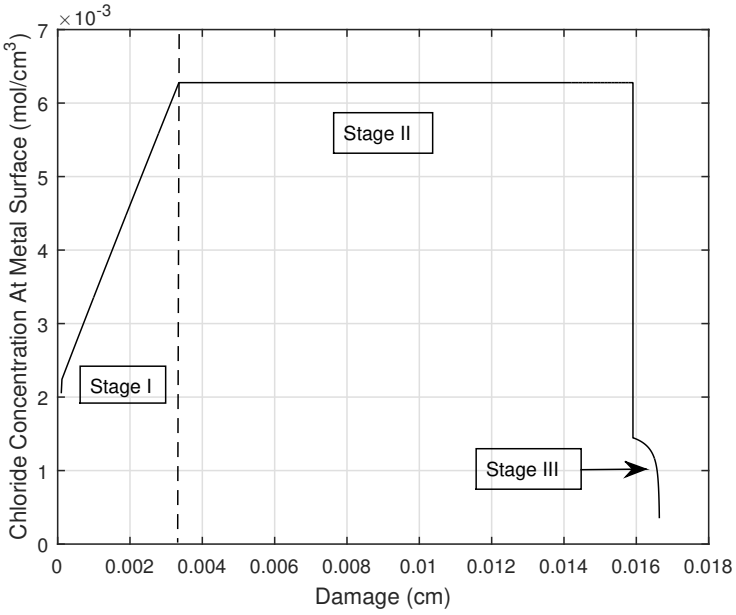

Figure 4.26: Chloride concentration at the metal interface (z = h) versus pit depth z through the end of Stage III.

We now describe how changing the scan rate s and the bulk value of potential E_B, and the bulk value of chloride affects the model results.

The scan rate s for Stage III can be used to to control the total damage h. Using $5\,mV/s$ as our baseline scan rate, we recorded the damage for Stage III and the overall pit damage for the simulation. We then arbitrarily decreased the scan rate and reran the simulation, recording both the Stage III damage and the overall damage. This procedure was done until we had obtained results for four different scan rates, which are displayed in Table 4.1. It is clear from the table that shorter scan rates produce pits that are deeper and require a longer time to reach repassivation. We plotted the total damage for Stage III versus the inverse scan rate, and were then able

to fit the data using a simple linear curve fit $h = 3.2103\left(\frac{1}{s}\right) + 2.7533$. This gives an easy way to predict the scan rate needed to produce a given pit depth. For example, if we wish for the damage from Stage III to be $h = 500\,\mu m$, (and hence the total pit depth is $659.07\,\mu m$) then our fit gives us the needed scan rate of $s = 0.006456\,mV/s$.

Table 4.1: The effect of scan rate s on total pit damage h.

Scan Rate	Stage III Damage	Total Pit Damage
$5\,mV/s$	$7.29\,\mu m$	$166.36\,\mu m$
$1\,mV/s$	$34.87\,\mu m$	$194.04\,\mu m$
$0.2\,mV/s$	$166.94\,\mu m$	$326.01\,\mu m$
$0.1\,mV/s$	$321.99\,\mu m$	$481.06\,\mu m$

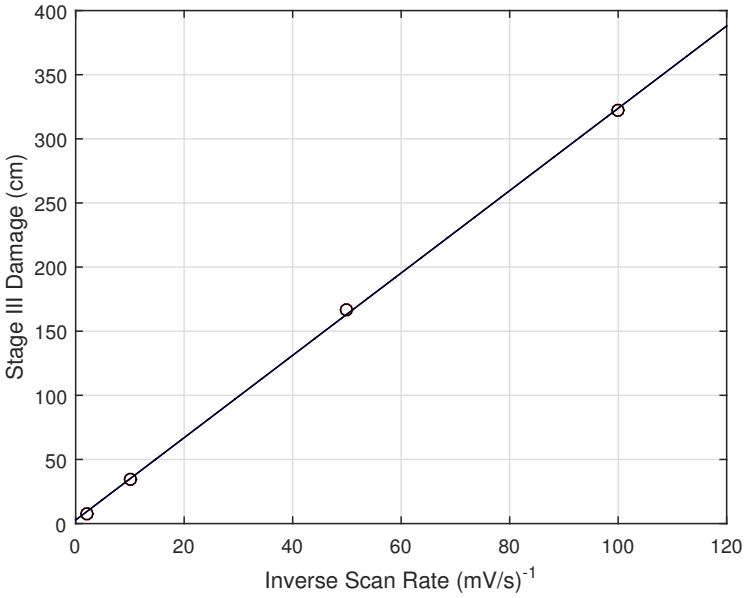

Figure 4.27: Total damage h in Stage III versus inverse scan rate $\frac{1}{s}$ and linear curve fit.

According to Frankel et al. in [15], if the bulk value E_B is increased, the current density i_A may also be increased. In our simulation, the value of i_A is user defined based upon an order of magnitude estimate, so it does not increase with E_B. When we increase the bulk value E_B, the potential curve for Stage I of the simulation is also increased. This causes our calculated value of E_{Hold} to increase, which is the potential value at the end of Stage I and the potential that we use for the potentiostatic hold in Stage II. Note however, that our calculated values for E_T and E_{RP} will not change. Because E_{Hold} has increased, it takes a longer amount of time to scan the potential in Stage II so that E reaches E_T, which increases the overall pit damage. Additionally, our calculated value for i_T is decreased, because

i_L is inversely proportional to h through (3.9). For example, increasing the bulk value from $E_B = 0.510\,V$ to $E_B = 1.0\,V$ results in $E_{Hold} = 0.9402\,V$, the ending potential in Stage I. The total time for the simulation increases from 462 seconds to 559 seconds, and the damage increases from $167.27\,\mu m$ to $184.20\,\mu m$. The transition value decreases from $i_T = 0.5214\,\frac{A}{cm^2}$ to $i_T = 0.4692\,\frac{A}{cm^2}$ We also note that if we increase E_B, our polarization curve will no longer match the curve of Srinivasan et al. [16] because i_L is smaller and the potentiostatic hold in Figure 3a [16] is done using a larger E_{Hold}.

A similar result can be said for decreasing the value of E_B. Decreasing E_B causes E_{Hold} to decrease, and the time to scan the potential in stage II is decreased, resulting in the total damage to decrease and i_L to increase. For example, if we decrease the bulk value from $E_B = 0.510\,V$ to $E_B = 0.350\,V$, the total time for the simulation decreases from 462 seconds to 430 seconds, and the damage decreases from $166.36\,\mu m$ to $160.22\,\mu m$. The transition value increases from $i_T = 0.5214\,\frac{A}{cm^2}$ to $i_T = 0.5426\,\frac{A}{cm^2}$.

Finally, we note that the shape of the polarization curve $i(E)$ is dependent upon the value of the bulk chloride. While we currently have the ability to determine how changing Cl^-_{Bulk} could affect our results, we need polarization curves for different bulk chloride concentrations. To our knowledge, the only polarization curve $i(E)$ for stainless steel that is plotted with clear values of E_T and E_{RP} is in the model by Srinivasan et al. [16]. If more data become available, then we can make a more extensive study on the effect of Cl^-_{Bulk}.

4.2 Summary of Findings

We now present a summary of our findings. The following is a full list of the assumptions that we make in the model:

- Metastable growth in Stage I is ohmic controlled and varies linearly in time. The current density is constant and large.
- Stable growth in Stage II is diffusion controlled and varies according to the square root of time.
- Stable growth in Stage III is ohmic controlled and the depth will asymptotically reach its maximum value at a rate that is slower than the square root of time. The current density is chosen to be a decreasing function of potential.
- Hydrolysis and other bulk reactions are neglected, assuming all are in equilibrium, so we only consider the species Fe^{2+}, Na^{+} and Cl^{-}.
- We only consider pits with width w and depth h such that $w << h$ so we may use a thin domain asymptotic expansion and pit growth is unidirectional.
- The solid domain is homogeneous and the concentration of metal ions is a constant value $C = C_{solid}$ at all time [12].
- Mass transport can be due to diffusion or electromigration from a potential gradient; however, advection is neglected.

- The concentration of ions within the electrolyte is in quasi-steady state. The term quasi-steady refers to the fact that the rate of diffusion is much faster compared to the rate of dissolution, however the pit depth h is still a function of time.

- Electromigration can be neglected in the diffusion controlled regime, so that each ionic species is a linear function of pit depth.

- A polarization curve is known, including the values for E_B, E_{Pit}, E_T, i_T, E_{RP} and i_{RP}.

- The values for MW and ρ are known for the alloy, as well as the values i_A, Cl_{bulk}, Na_{bulk}, C_{bulk}, C_{Solid}, and C_{sat}.

As long as the assumptions above are true, we have found the following results to hold:

1. The required damage h to reach a specified current density i_A can be predicted by equating the Stage II growth rate with the growth rate as described by Faraday's Law. As shown in (3.8), the predicted damage h is inversely proportional to the specified current density i_A.

2. The diffusion limiting current density i_L is inversely proportional to the damage h, where the slope is dependent upon the concentration values C_{bulk}, C_{Solid}, and C_{sat}, as well as the diffusivity of the metal ions D. This is shown by the results (3.9) and (3.10).

3. The square of the diffusion limiting current density i_L^2 is inversely proportional to the time t, where the slope is dependent upon the concentration values C_{bulk}, C_{Solid}, and C_{sat}, as well as the diffusivity of the metal ions D. This is shown by the results (3.14) and (3.15).

4. We can choose the diffusivity of the metal ions D to match a known slope for a graph of i_L versus $\frac{1}{h}$, or a graph of i_L^2 versus $\frac{1}{t}$.

5. We can approximate the slope of the graph of i_L^2 vs $\frac{1}{t}$ by the quantity $2DF^2C_{Solid}\gamma C_{sat}$.

6. The potential drop ΔE in the diffusion controlled regime is a constant that depends upon the bulk values Na_{bulk} and Cl_{bulk} as well as the saturation level of the metal C_{sat}, as shown in (2.38).

7. The damage h can be accurately curve fit to the power law at^b if the Stage III data is truncated at the end of the early time growth phase.

8. The scan rate s for Stage III can be used to control the total damage h. Shorter scan rates produce pits that are deeper and require a longer time to grow.

9. If the bulk value E_B is increased, the calculated E_{Hold} is increased, as well as the overall pit damage and the time required to scan the potential in Stage II. The calculated transition current density i_T is decreased. Similar results hold if E_B is decreased.

Our results (2.38), (3.10) and (3.15), as well as the overall pit depth for the model and the plot of the chloride concentration at the metal interface were all verified against

experimental results. Our analytic expression for the potential drop (2.38) verified the observation by Laycock [4] that the potential drop in the diffusion controlled regime was constant. The slope in (3.10) was able to reproduce the value reported by Srinivasan et al. [16] in Figure 7a [16] and the slope in (3.15) was able to reproduce the value reported by Moayad et al. [13] in Figure 4 [13]. Our overall pit depth at the end of Stage III matched the reported pit depth by Srinivasan et al. [16] in Figure 7a [16]. Our plot of the chloride concentration at the metal interface was able to reproduce the general trend that is displayed in Mankowski et al. [21] in their plot of chloride concentration versus pit diameter (Figure 1 [21]).

It is also important to note that the scan rate s is able to control the damage h for a fixed polarization curve. If we had chosen to increase or decrease the length of the potentiostatic hold in Stage II to alter the pit depth, this would also affect the calculated value of i_T. For example, if we increased the length of the potentiostatic hold, the pit depth would increase and i_T would decrease.

Finally, note that the result number (6) in our findings list has important implications for the future creation of Markov Models that can predict damage evolution by using input parameters a and b from the growth model $h(t) = at^b$. This is discussed more when we describe future work in Chapter 5.

CHAPTER V

FUTURE WORK

5.1 Future Work

The most immediate use for our pit growth model is to incorporate it into existing Markov Models [22], which stochastically predict damage evolution of a pit based on different environmental parameters. These next generation Markov Models will predict damage evolution by using input parameters a and b in the growth model $h(t) = at^b$. It is currently somewhat known how a and b are affected by environmental conditions including potential, pH, and chloride and pollutant concentrations as well as how a and b depend on pH and temperature for common metals [23, 24, 25, 26]. By correlating known field data for the needed environmental conditions with a curve fit using our power law, we will be able to generate a and b which can then be used in the Markov Model. Another intended use of the results is to use them for creating a new 3D stochastic model by building upon the model of Pieter Van der Weeën et al. [3] which uses cellular automata to simulate pit growth. To improve the model, the pit initiation stage will be amended to better accomodate for the influence of spatial variation in potential and chloride concentration. The "diffusion scheme" will be updated to allow for increased chloride transport into the pit to better account

for the effects of electroneutrality. Finally, the pit growth model will be improved to better account for the influence of pH and temperature on pit depth. This thesis will be used to help create a set of guidelines for pit growth and as a baseline result to compare with the results of the cellular automata model.

While our model is able to successfully create accurate power law models for pit propagation in the form $h(t) = at^b$, this approach is limited by the requirement of the user to have a substantial amount of data in their posession including the four defining values of potential E_{Bulk}, E_{Pit}, E_T, and E_{RP} on a polarization curve $i(E)$ as well as the bulk chloride value Cl^-_{Bulk}, the saturation level of metal ions C_{sat}, and an initial current density i_A for production of metastable pits. As more pit data become available, our model can be verified for additional polarization curves which we hope can improve its overall accuracy and streamline the model to require fewer input parameters. There are also many natural ways that our model can be improved in future research. For example, we could create a two dimensional model assuming that the width and depth are close to the same order of magnitude so that we could incorporate more complex geometries, or we could model a more realistic pit chemistry by incorporating bulk reactions.

BIBLIOGRAPHY

[1] G. S. Frankel. Pitting corrosion of metals: A review of the critical factors. *Journal of The Electrochemical Society*, 145(6):2186–2198, June 1998.

[2] J. R. Galvele. Transport processes and the mechanism of pitting of metals. *Journal of The Electrochemical Society*, 123(4):464–474, April 1976.

[3] P. Van der Weeën, A. M. Zimer, E. C. Pereira, , L. H. Mascaro, O. M. Bruno, and B. De Baets. Modeling pitting corrosion by means of a 3d discrete stochastic model. *Corrosion Science*, 82:133–144, 2014.

[4] N. J. Laycock and R. C. Newman. Localised dissolution kinetics, salt films and pitting potentials. *Corrosion Science*, 39(10-11):1771–1790, 1997.

[5] British stainless steel association. `http://www.bssa.org.uk/faq.php`, 2007 (accessed February 18, 2016).

[6] G. S. Frankel. Advances in localized corrosion. In *NACE, Houston*, page 137, 1990.

[7] K. J. Vetter and H. H. Strehblow. Localized corrosion. In *NACE, Houston*, page 240, 1974.

[8] G. T. Gaudet, W. T. Mo, T. A. Hatton, J. W. Tester, J. Tilly, H. S. Isaacs, and R. C. Newman. Mass transfer and electrochemical kinetic interactions in localized pitting corrosion. *American Institute of Chemical Engineers*, 32:949–958, June 1986.

[9] Z. Y. Chen and R. G. Kelly. Computational modeling of bounding conditions for pit size on stainless steel in atmospheric environments. *Journal of The Electrochemical Society*, 157(2):C69–C78, 2010.

[10] A. Anderko, N. Sridhar, and D. S. Dunn. A general model for the repassivation potential as a function of multiple aqueous solution species. *Corrosion Science*, 46:1583–1612, 2004.

[11] D. D. Macdonald and G. R. Engelhardt. Chapter predictive modeling of corrosion. In B. Cottis, M. Graham, R. Lindsay, S. Lyon, T. Richardson, D. Scantleburn, and H. Stott, editors, *Schreir's Corrosion*, volume 2, pages 1630–1679. Elsevier, Amsterdam, 2010.

[12] R. Duddu. Numerical modeling of corrosion pit propagation using the combined extended finite element and level set method. Technical report, Vanderbilt University, April 2014.

[13] M. H. Moayed and R. C. Newman. Using pit solution for evaluation of metastable pitting stability of austenitic stainless steel. *Materials and Corrosion*, 56(3):166–173, 2005.

[14] N. J. Laycock and R. C. Newman. Temperature dependence of pitting potentials for austenitic stainless steels above their critical pitting temperature. *Corrosion Science*, 40(6):887–902, 1998.

[15] G. S. Frankel, L. Stockert, F. Hunkeler, and H. Boehni. Metastable pitting of stainless steel. *National Association of Corrosion Engineers*, 43(7):429–436, 1987.

[16] J. Srinivasan, M. J. McGrath, and R. G. Kelly. A high-throughput artificial pit technique to measure kinetic parameters for pitting stability. *Journal of the Electrochemical Society*, 162(14):C725–C731, 2015.

[17] J. Srinivasan, M. J. McGrath, and R. G. Kelly. Mass transport and electrochemical phenomena influencing the pitting and repassivation of stainless steels in neutral chloride media. *ECS Transactions*, 58(31):1–11, 2014.

[18] J. W. Tester and H.S. Isaacs. Diffusional effects in simulated localized corrosion. *Journal of The Electrochemical Society*, 122(11):1438–1445, 1975.

[19] H. S. Isaacs. The behavior of resistive layers in the localized corrosion of stainless steel. *Journal of The Electrochemical Society*, 120(11):1456–1462, 1973.

[20] M. A. Bright. *Dissolution and Diffusion Characteristics of 316L Stainless Steel in Molten Zinc Containing Variable Concentrations of Aluminum.* PhD thesis, West Virginia University, 2007.

[21] J. Mankowski and Z. Szklarska-Smialowska. Studies on accumulation of chloride ions in pits growing during anodic polarization. *Corrosion Science*, 15:493–501, 1975.

[22] K. McCallum, J. Zhao, M. Workman, M. Iannuzzi, M. Kappes, J. Payer, C. B. Clemons, S. Chawla, K. L. Kreider, N. Mimoto, and G. W. Young. Localized corrosion risk assessment using Markov analysis. *Corrosion*, 70(11):1114–1127, November 2014.

[23] F. Caleyo, J. C. Velazquez, A. Valor, and J. M. Hallen. Markov chain modeling of pitting corrosion in underground pipelines. *Corrosion Science*, 51:2197–2207, 2009.

[24] M. K. Cavanaugh, R.G. Buchheit, and N. Birbilis. Modeling the environmental dependence of pit growth using neural network approaches. *Corrosion Science*, 52:3070–3077, 2010.

[25] M. K. Cavanaugh, N. Birbilis, and R. G. Buchheit. Modeling pit initiation rate as a function of environment for aluminum alloy 7075-t651. *Electrochimica Acta*, 59:336–345, 2012.

[26] J. C. Velazquez, F. Caleyo, A. Valor, and J. M. Hallen. Predictive model for pitting corrosion in buried oil and gas pipelines. *Corrosion*, 65:332–342, 2009.

[27] S. M. Sharland, C. P. Jackson, and A. J. Diver. A finite-element model of the propagation of corrosion crevices and pits. *Corrosion Science*, 29(9):1149–1166, 1989.

[28] M. D. Brackman. Modeling and simulation of damage evolution in crevice corrosion. Master's thesis, The University of Akron, August 2012.